Diogo Farias Gonçalves Alexandre Rodrigues

Licenciado em Ciências da Engenharia

Plasma Nitriding of AA2011 Alloy and Surface Characterization by NDT Techniques

Dissertação para obtenção do Grau de Mestre em

Engenharia Mecânica

Orientador: Doutor Telmo Santos, Professor Auxiliar,

Universidade Nova de Lisboa

Co-orientadores: Doutora Rosa Miranda, Professora Associada com Agregação,

Universidade Nova de Lisboa

Doutor Tatsuhiko Aizawa,

Shibaura Institute of Technology, Tóquio

FACULDADE DE CIÊNCIAS E TECNOLOGIA
UNIVERSIDADE NOVA DE LISBOA

Setembro 2015

Plasma Nitriding of AA2011 Alloy and Surface Characterization by NDT Techniques

Faculdade Ciências e Tecnologia, Universidade Nova de Lisboa

AGRADECIMENTOS

Gostaria de agradecer ao meu orientador, o Prof. Telmo Santos, por me aceitar como orientando, por partilhar os seus conhecimentos na área dos ensaios não-destrutivos mas sobretudo por me motivar durante estes seis meses de investigação. Gostaria também de agradecer à minha co-orientadora, a Prof.ª Rosa Miranda, por ter sempre tempo para me ajudar, mesmo à distância, e por ter revisto a minha tese tantas vezes.

Não esquecendo os meus mentores e colegas do Japão, um muito obrigado ao Prof.Aizawa, ao Morita-san, ao Edo Yunata e ao Kurozumi-san por me terem acolhido em Tóquio e por me terem ensinado tudo o que sei sobre processos plasma.

Obrigado ao Patrick Inácio que, apesar de nos conhecermos pouco, perdeu quatro dias a fazer ensaios de condutividade só para mim.

Um obrigado e um beijinho à Carolina que teve força e paciência para esperar por mim.

Um grande, grande obrigado à minha mãe que esteve comigo todos os dias, apesar de estar a 11.151 quilómetros de distância.

Por último gostaria de agradecer ao Shibaura Institute of Technology, pela bolsa de estudo, e à Fundação para a Ciência e a Tecnologia (FCT, I.P.), pelo suporte financeiro concedido no âmbito do projeto INSPECT (PTDC/EEI-PRO/3219/2012).

ACKNOLEDGEMENTS

I would like to thank my advisor, Prof. Telmo Santos, for taking me as his advisee, for sharing his knowledge in the field of non-destructive testing, but above all for keeping me motivated during these six months of research. I would also like to thank my co-advisor, Prof. Rosa Miranda, for always taking the time to help me and for revising my thesis so many times.

Not forgetting my mentors and colleagues in Japan I must send a word of thanks to Prof.Aizawa, Morita-san, Edo Yunata and Kurozumi-san. Thank you for receiving me with open arms and for teaching me everything I know about plasma treatments.

Thank you, Patrick Inácio, for taking four days to do conductivity tests with me, even though we do not know each other well.

A thank you and a kiss to Carolina for having the strength and the patience to wait for me.

The biggest thank you to my mother for having been with me everyday, even though she was 11.151 kilometers away.

Lastly I would like to thank the Shibaura Institute of Technology, for the scholarship, and Fundação para a Ciência e a Tecnologia (FCT, I.P.), for the financial support granted under the project INSPECT (PTDC/EEI-PRO/3219/2012).

RESUMO

As ligas Al-Cu são frequentemente utilizadas nas industrias aeroespacial e automóvel pois possuem elevada resistência específica, especialmente em algumas condições de tratamento térmico. Contudo, devido a problemas de corrosão e desgaste, são normalmente anodizadas e pintadas. A nitruração por plasma foi proposta como alternativa, ainda que atualmente se encontre num estado pouco avançado de desenvolvimento para as ligas de Al.

As técnicas de caracterização elétrica estão bem implementadas na indústria enquanto técnicas de NDT devido à sua boa precisão associada a um baixo custo, relativamente a outros ensaios não-destrutivos. Algumas destas técnicas, como as correntes induzidas e as sondas de 4 pontos, são regularmente utilizadas em inspeções de revestimentos superficiais.

Esta tese teve como objectivo fazer nitruração por plasma a baixa temperatura de alumínio de modo a reduzir o impacto no tratamento de revenido inicial, bem como, estudar a possibilidade de utilização de correntes induzidas na caracterização das superfícies nitruradas.

O trabalho de investigação foi feito em duas fases. A primeira consistiu na calibração do processo e foi feita no Shibaura Institute of Technology, em Tóquio. A segunda consistiu na caracterização elétrica das amostras e foi feita no laboratório de ensaios não destrutivos, na Faculdade de Ciências e Tecnologia da UNL.

As amostras da liga AA2011 foram nitruradas com sucesso a baixa temperatura e foi encontrada uma relação entre as medições de *lift-off* das correntes induzidas e as propriedades do revestimento.

ABSTRACT

Al-Cu alloys are widely used in the aerospace and automotive industries due to their high specific strength in some tempered conditions. However, due to poor corrosion and wear resistance, they are often anodized and/or painted. Plasma nitriding has been proposed as an alternative, though the developments in this technique are still in a recent stage for Al alloys.

Electrical characterization techniques are well implemented NDTs in the industry because of good accuracy associated with lower cost, compared to other methods. Some, like eddy currents and 4-point probe techniques, are often used in coating inspection.

The objective of this study was to perform Al nitriding at low temperatures to minimize the tempering initial condition damage and to assess the feasibility of eddy currents technique as a method for evaluating surface properties.

The work developed can be divided in two stages. The first one was the process tuning, done at the Shibaura Institute of Technology, in Tokyo; and the second was the electrical characterization done in Faculdade de Ciências e Tecnologia, UNL.

Low temperature nitriding of AA2011 alloy specimens was successfully achieved. Electrical conductivity results show that *lift-off* measurements by eddy currents testing can be related to surface properties.

KEY WORDS

Aluminum nitriding, Electrical characterization, Non Destructive Testing, Eddy Currents

CONTENTS

LIST OF FIGURES

LIST OF TABLES

1. INTRODUCTION

1.1. Motivation

Aluminum is a material with great potential for many industrial applications. It offers an interesting combination of properties in alloy form, such as light weight, high strength and good general workability. These characteristics make it attractive for use in fields such as aerospace, automotive, railway and marine. Aluminum increases its strength as temperature decreases, and thus it is suitable for cryogenic purposes such as in pressure vessels and space technology. It is resistant to corrosion due to the thin oxide film that forms on its surface after contact with air moist.

In spite of these attractive properties, aluminum has poor mechanical surface properties that lead to high wear and, in some alloys, to high corrosion. Surface enhancing technologies are standard in modern industries. Tribological properties of several metals can be improved by processes such as carburizing, nitriding, boriding, anodizing, chemical vapor deposition, electroplating, etc. Surface properties of aluminum are usually enhanced by anodizing though it produces some problems like high porosity and high wear. An alternative to anodizing is Nitriding. Nitriding forms a surface layer of aluminum nitride that has high hardness and high corrosion and wear resistances. Aluminum nitride has an advantage over aluminum oxide in marine applications because it passivates and does not dissolve by reaction with chloride. However, because aluminum nitriding is still fairly recent, process parameters and nitride formation mechanisms are still not entirely understood.

Overall, the state-of-the-art in what concerns aluminum plasma nitriding is very promising but, in order to obtain a large scale industrially applicable process, additional research is paramount.

This was a joint work between the Non-Destructive Testing (NDT) laboratory of the Department of Mechanical and Industrial Engineering of FCT and the Nano-Film and Coating (NFC) laboratory of the Department of Engineering and Design of the Shibaura Institute of Technology (SIT). The knowledge and equipment available at both the NDT and NFC laboratories made this work possible.

1.2. Objective

This work aims to contribute to a further understanding of the plasma nitriding process, in order to make it significantly superior and reliable for industrial applications in aluminum alloys. In this specific case, nitriding of alloy AA2011 was studied, as well as the parameters that produce the most uniform and smooth coatings. Since most aluminum alloys are hardened and tempered, nitriding was performed at low temperature which was innovative for Al alloys.

The eddy currents technique is proposed as a non-destructive test to determine the characteristics of this type of diffusion coating. Ideally it will be able to describe the nitride layer in terms of thickness, concentration gradient and hardness.

1.3. Thesis Structure

This thesis is structured in 6 chapters. The first contains the motivation and the objectives of the work. Chapter 2 describes the state-of-the-art in plasma nitriding of aluminum alloys, including the techniques employed and the current understanding of the nitriding mechanisms.

Chapter 3 presents the state-of-the-art in eddy currents testing, as well as the basics and fundamentals of the method.

In chapter 4, the materials, equipment and experimental procedure are described.

In chapter 5 the nitriding results are presented and discussed. This includes preliminary inspection of the nitrided samples, analysis of the conductivity and hardness tests and preliminary conclusions.

Finally, chapter 6 draws the final conclusions and suggests topics for future research on this subject.

2. NITRIDING OF ALUMINUM ALLOYS

This chapter provides an overview of the existing methods for improving surface performance of the 2xxx series alloys, in terms of surface hardness, corrosion and wear.

A brief introduction to aluminum alloys is given, followed by a description of plasma nitriding principles and techniques.

2.1. Aluminum and its alloys

Aluminum occurs near the Earth's surface in deposits of bauxite, usually tightly combined with oxygen and silicon. In Earth's crust, it is the third most abundant element (8%), surpassed only by oxygen (47%) and silicon (28%), and the most abundant metal. The difficulty of extracting aluminum from its natural deposits raises its cost relatively to some less plentiful metals but its unique set of characteristics make attractive to many industries.

In its pure form, aluminum is very resistant to most types of corrosion, it has high thermal conductivity ($205\ Wm^{-1}K^{-1}$ at $25ºC$) and it is easy to fabricate by conventional methods, such as extruding, bending, drawing, etc. It has excellent electrical conductivity but very low strength ($10\ MPa$) and hardness ($17\ HV$). It is reflective, non-toxic and easy to recycle. Low strength and low hardness keep it from being used in structural applications or in abrasive conditions. These issues are addressed by alloying it with other elements although, most of the times, other characteristics such as corrosion resistance and electrical conductivity are reduced. In some cases, surface treatments might be required.

Aluminum alloys are widely used in industries such as aerospace, automotive, marine, electrical and others; in components where high strength combined with corrosion resistance are a requirement. Alloying involves adding a certain percentage (usually less

than 10% in total) of copper, magnesium, manganese, silicon, tin, zinc and others, to modify the properties of aluminum in a desired way, given that only some elements effectively increase the mechanical properties.

Aluminum alloys are divided into two classifications: casting alloys, those that are melted and poured into a mold; and wrought alloys, those that are worked mechanically in the solid state. Cast alloys contain higher percentages of alloying elements resulting in a more heterogeneous structure and, generally, lower ductility in comparison to wrought alloys.

Wrought alloys are the most used in the aforementioned industries because of their higher melting point and tensile strength. Aluminum alloys increase their strength by cold working but only some have a significate response to heat treatments, therefore, they are subdivided into heat-treatable and non-heat-treatable.

2xxx

The 2xxx series are a heat treatable series in which copper is the primary alloying element, giving them high strength but little corrosion resistance. They were widely used in the aerospace industry but, because of weldability, machinability, wear and corrosion issues, they have been replaced by alloys of the 7xxx series in many applications. They are heat treatable because of their high copper content which makes them unsuitable for fusion welding processes. Solid state welding is the most adequate for these alloys and therefore welding is limited to certain part geometries and joint configurations.

2.1.1. Precipitation Hardening

Precipitation hardening consists on the formation of coherent precipitates of solute atoms, that is, precipitates with the same crystal structure as the parent phase. Strengthening and hardening of an alloy occur because dislocations are anchored or trapped when they reach a coherent precipitate. This is due to the increased strain originated by differences in size between solute and solvent atoms, which compensates for the decrease in strain associated with dislocations. If a precipitate is incoherent (forming a disordered interface with the matrix, like a grain boundary) or semicoherent (forming a dislocation-containing interface with the matrix) it will not increase hardness and strength effectively because dislocations will circumvent it.

Although most binary aluminum alloy systems form precipitates, not all of them have a significant response to heat treatments. The composition and concentration of the precipitates are the main factors that contribute to the strength of an alloy. The systems that respond better are the aluminum-copper, the aluminum-copper-magnesium, the aluminum-magnesium-silicon and the aluminum-zinc-magnesium-copper. In order to understand the basic principles of precipitation hardening, let us study the simpler of systems, the binary aluminum-copper system. Fig. 1 shows the Al-Cu phase diagram, typical of the 2xxx series alloys.

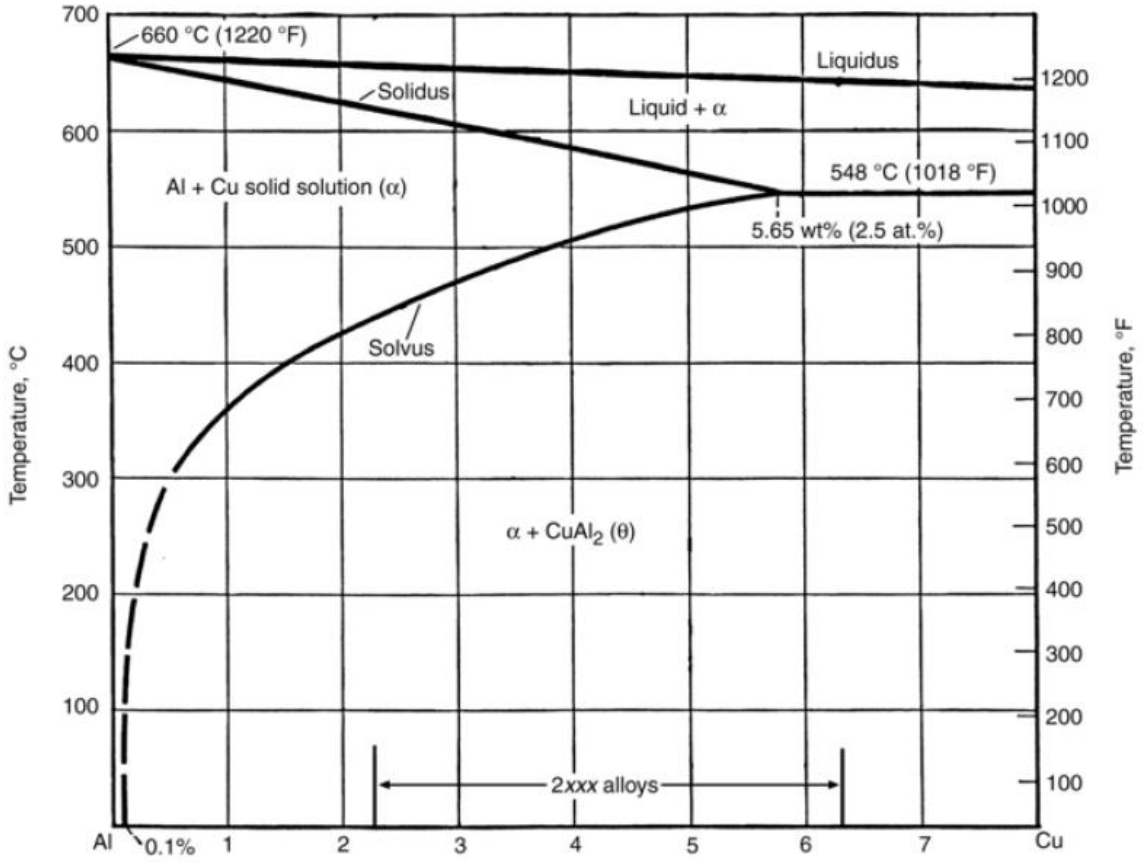

Fig. 1 – Aluminum rich section of the Al-Cu phase diagram. [1]

Let us consider an alloy with $4\%w$ copper at $550℃$ where a single phase (α) aluminum and copper solution exists. If it is cooled slowly, Al_2Cu precipitates (θ), which are incoherent precipitates, will form and the alloy will not have increased hardness or strengthen - it is said to be in its *annealed* state. However, if it is cooled rapidly to room temperature (quenched), diffusion will not occur and θ precipitates will not form. The crystal structure of the α phase will be preserved, though it will be supersaturated with copper and unstable.

After quenching, the alloy will go through what is called aging or precipitation hardening, as in the example shown in Fig. 2. At a temperature well below the *solvus* line, in solute-rich regions designated Guinier-Preston (GP) zones, coherent Al_2Cu precipitates (θ'') start to form initially lowering strength due to a lowering of the copper content of the matrix (1). Afterwards, as these coherent precipitates grow in the GP zones, strength increases (2). Intersections between precipitates and dislocations further increase hardness (3) until a peak is reached when incoherent θ precipitates start to form (4) and the alloy starts to anneal.

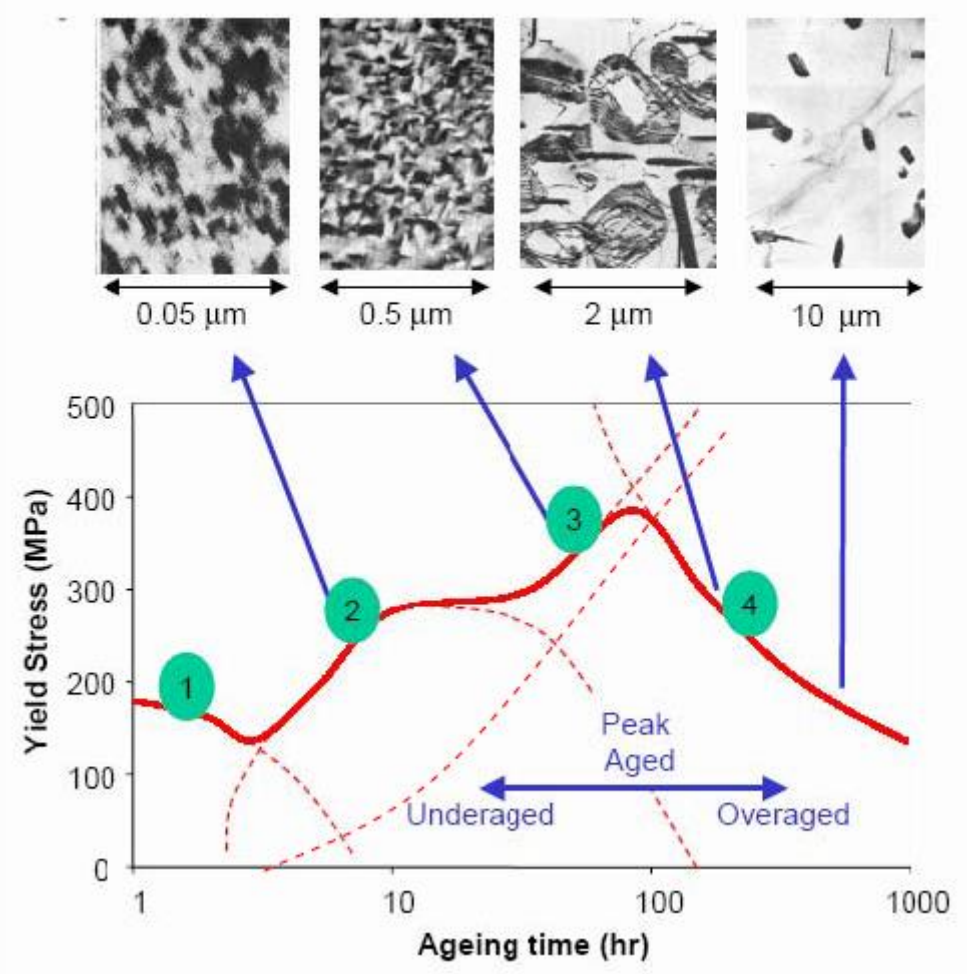

Fig. 2 – Effects of aging time in microstructure and yield strength of low copper Al-Cu alloys.

An aged alloy that has not yet reached its peak hardness is called underaged, while an alloy that has surpassed this peak is called overaged. Overaging will lead to partial or full annealing.

Aging occurs naturally at room temperature but it can also be controlled artificially by controlling treatment temperature and holding time. Fig. 3 shows the typical temperature

ranges for solution heat treatments, annealing and artificial aging in an aluminum copper system. Fig. 4 correlates the processing temperature and time with the resulting yield strength for an AA2024 alloy. Understanding aging is very important in alloy selection in order to take full advantage of the enhanced characteristics of the 2xxx series alloys.

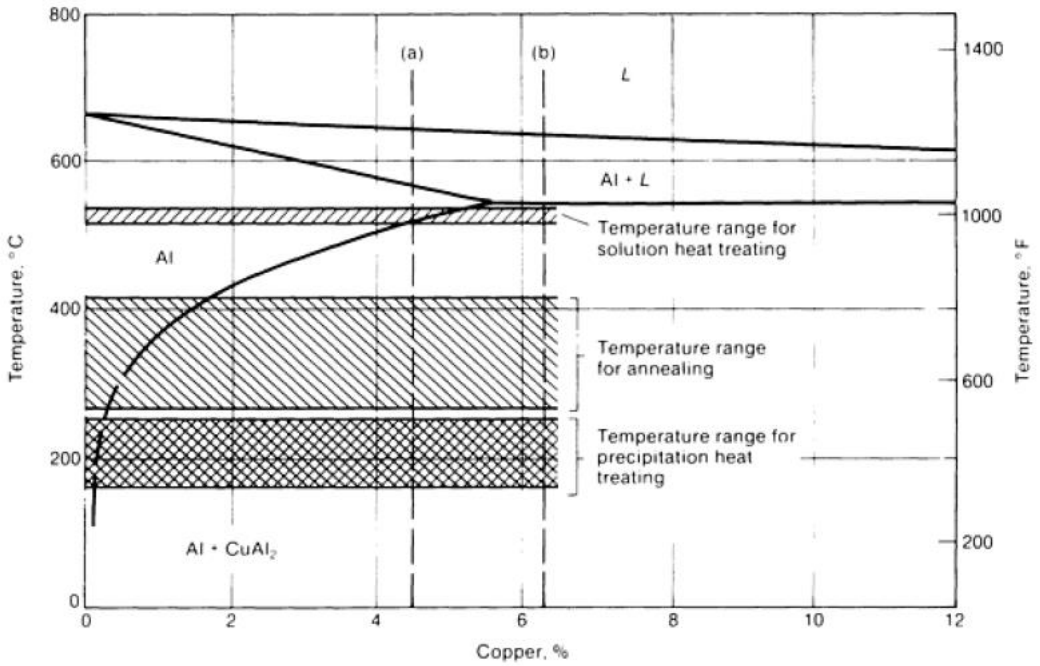

Fig. 3 – Al-Cu phase diagram showing temperature ranges for solution heat treating, annealing and precipitation hardening. [2]

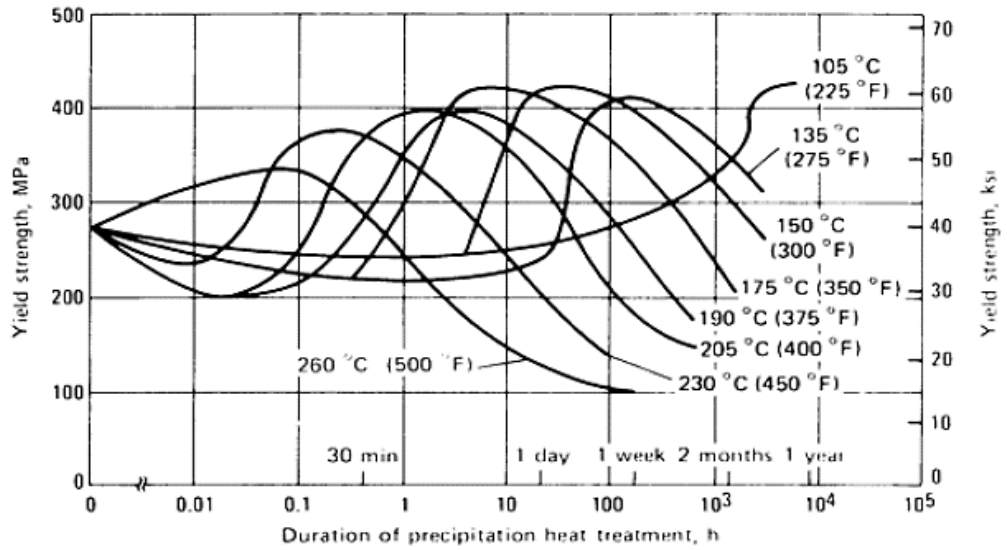

Fig. 4 – Relationship between resulting yield strength, holding time and temperature in artificial aging of a 2024 alloy. [2]

2.2. Corrosion Resistance

Corrosion resistance is one of the most important properties of materials when it comes to determining the service life of a component. It depends on the composition of the material, and on the strength, electric current, temperature and environment to which a component is subjected to. Most aluminum alloys are less corrosion resistant than pure aluminum. General corrosion resistance is usually an inverse function of copper content and, therefore, the 2xxx series are the least corrosion resistant alongside some alloys of the 7xxx series. Other alloying elements like lead, nickel and tin also tend to decrease corrosion resistance though to a smaller extent.

Though the mechanisms involved at a microscopic level are the same, at a macroscopic level corrosion can manifest in different forms, such as galvanic corrosion, pitting corrosion, crevice corrosion and Stress Corrosion Cracking (SCC).

The 2xxx series alloys are more prone to corrosion because they contain copper, which precipitates in the form of Al-Cu particles, and some contain copper and magnesium, which precipitate in the form of Al-Cu-Mg particles. The area involving each of these is a propitious site for pit initiation because they are cathodic to the matrix (Al-Cu-Mg particles are initially anodic but they become cathodic due to dealloying). During dissolution of the Al-Cu(-Mg) particles, regions with metallic copper are formed in the matrix, thereby contributing to further galvanic corrosion and sustaining the pit growth.

These precipitates also make the alloy more susceptible to intergranular corrosion (IG) and SCC, though this susceptibility can vary significantly with copper content and temper conditions. Slow quenching makes the alloy susceptible to IG corrosion, while rapid quenching makes more susceptible to SCC because of bigger precipitates.

2.3. Nitriding

Nitriding is a surface hardening heat treatment that consists of introducing nitrogen into the surface of a metal component. Steel alloys are the most common materials to be nitrided but other metals, as well as non-metals, can also be treated. In fact, the process is dependent on the presence of strong nitride forming elements such as aluminum, chromium, molybdenum, vanadium and tungsten.

Nitrogen can be delivered to the surface of a component by three different donors: gas, salts and ions.

In gas nitriding, a nitrogen rich gas, usually ammonia (NH_3), delivers nitrogen to the surface of a component. Inside a gas filled chamber, components are heated in order to supply energy to the ammonia molecules. These dissociate into hydrogen and nitrogen and the latter penetrates the surface to create a nitride layer. Gas nitriding is the oldest and simplest of the three and it has been used for almost a century on steel alloys.

In salt bath nitriding, components are heated and dipped in a tank filled with a bath containing cyanides or cyanates. It is a much simpler process than gas nitriding but has a narrower range of applications. Due to high toxicity of the salts it has been less used in the last decades in favor of cleaner technologies.

In ion nitriding, as the name suggests, nitrogen is delivered to the surface of a component in the form of ions generated in a plasma. In addition to a heat source to heat samples, it requires electronic control and electric power supply to generate and sustain the plasma. Nevertheless, in general, it has the lowest power consumption of the three. Unlike gas nitriding, it works with lower gas pressures and consequently has lower gas consumption. Unlike salt bath nitriding it does not utilize nor produce toxic substances.

In the case of aluminum, nitriding involves substituting the aluminum oxide (Al_2O_3) layer for aluminum nitride (AlN). Early attempts have lead to thickness irregularity, detachment and contamination of the nitride layer, mainly due to the presence of Al_2O_3 acting as a barrier between metal and nitrogen and retarding the diffusion of nitrogen into the substrate. Complete removal of the alumina layer before nitriding and absence of O_2 during nitriding are paramount. As a result aluminum nitriding becomes a much more demanding process. There are several methods for removing the oxide layer: addition of magnesium, ball milling in a controlled atmosphere and sputtering.

Sputtering is a surface treatment that, like ion nitriding, involves plasma technology, hence, the two can be combined in a two-step process with only one equipment setup. Inside the same chamber, with minor parameter changes, the Al_2O_3 layer can be eliminated by pre-sputtering; and the AlN layer can be formed by nitriding.

Ion Nitriding

There are two main types of ion nitriding processes, Nitrogen Ion Implantation (NII) and Plasma Nitriding (PN), distinguishable by the main mechanism of ion introduction to produce case hardened layers.

Nitrogen Ion Implantation (NII) is a high energy, non-thermal, non-equilibrium, physically driven, ballistic alloying process. Concentrated in a beam, nitrogen ions accelerate towards the surface of a sample to bombard it with sufficient kinetic energy to produce a hardened layer. The layer is relatively shallow but very hard. The beam propagates in high vacuum at room temperature and is generated in an atomic particle accelerator. Surface hardening in mostly due to dislocation pinning.

Plasma Nitriding (PN), on the other hand, is a low energy, thermally driven, equilibrium, diffusion process. In a plasma created around a sample, nitrogen neutrals and ions react chemically with the surface atoms to create a nitride layer that grows by diffusion. The resulting layer is relatively deep but less hard than in NII. In PN the plasma usually has relatively low energy density and therefore components must be heated to facilitate the process. Surface hardening is mostly due to metal nitride precipitates [2].

NII has some limitations that make it less attractive from an industrial point-of-view. The ion beam has a small area of incidence so a surface has to be scanned several times to be completely nitrided. Processing large areas becomes unfeasible due to long processing times. Furthermore the beam should be nearly perpendicular to the surface which either imposes limits in component geometry and/or raises costs and processing times. Due to a general increase in geometric complexity of large scale fabricated parts, PN is a stronger option for industrial application [3]. The present study focuses on plasma nitriding exclusively.

2.4. Plasma Nitriding

Plasma technology and equipment setups used for aluminum nitriding are similar to the ones used for nitriding of steel alloys, as well as for many other industrial plasma processes such as sputtering, Physical Vapor Deposition (PVD) and plasma etching. However, because the mechanism of AlN formation and the influence of the many process parameters are not yet fully understood, this process is still in a very premature stage of development.

Many authors have reported to successfully nitride several aluminum alloys but all with different parameters and different results. For instance, a DC plasma study has reported a $10\ \mu\mathrm{m}$ thickness layer on an aluminum-titanium alloy [4] while another study that employed RF plasma reported a $4.5\ \mathrm{nm}$ thickness layer on a 2xxx series alloy [5], both with processing times in excess of $20\ \mathrm{h}$. An ECR study reported a very high thickness of $10\ \mu\mathrm{m}$ for a processing time of just $900\ \mathrm{s}$ [6] though extensive fusion of the substrate occurred, which is not desirable, especially in the case of heat-treatable aluminum alloys like the 2xxx and 7xxx series.

For this work a High Density Plasma (HD-Plasma) system, recently developed at SIT, was used to combine the more conventional DC- and RF-Plasma systems in order to mitigate each system's flaws. In this chapter a general process description is presented, then DC-, RF- and HD-systems are explained as well as process parameters for each case.

2.4.1. Plasma Generation

Plasma is usually described as the fourth state-of-matter, with some similarities to the gas phase and also some differences. It is a neutral medium of unbound positive and negative particles that interact with each other collectively in waves. Plasma is the most common phase of matter in the universe, present in lightning and in the nuclei of stars; it can also be generated artificially, such as in neon lamps and arc welding.

Artificial plasmas can be characterized by parameters such as the type of power source used to generate them, the pressure at which they operate, the degree of ionization, the temperature relationships within the plasma and the electrode configuration. For the purpose of this study two types of low-pressure non-thermal discharges will be described.

One way of generating artificial plasma is by applying a DC voltage between two electrodes surrounded by a dielectric gas. When the voltage reaches a certain value, the

gas (electrical insulator) ionizes transforming into plasma (excellent electric conductor) and producing a glowing light. This was the first method for producing artificial plasma and it is also known as *glow discharge*. It was the first low pressure discharge used to nitride aluminum [7] and , in the present work, it will be referred to as DC plasma.

Another way of generating artificial plasma is by supplying the gas with current produced by electromagnetic induction. This can be achieved by applying high radio frequency AC current on a coil placed outside the chamber that will create a time-varying magnetic field, which will in turns originate electric currents inside the chamber. This is called *Radio Frequency Inductively Coupled Plasma* (RFICP) and it has been used to successfully nitride aluminum alloys using an equipment setup referred to here as RF Plasma.

Higher frequencies (high RF or Microwave) are also used to generate plasma in low-pressure discharges called Wave Heated Discharges. For example, Electron Cyclotron Resonance (ECR) uses a microwave source in combination with a permanent magnetic field in order to ionize gas. It is used in the biomedical industry and it has been applied in plasma nitriding of pure aluminum [6].

DC Plasma

In DC plasma nitriding, there is a bias voltage between the chamber (anode) and the workpiece (cathode) that is responsible for both plasma generation (glow discharge) and ion acceleration. Fig. 5 shows an example of a DC setup. It is a very simple setup and it has less parameters than RF plasma but it has some disadvantages. There is a minimum bias voltage to create and sustain the glow discharge that is usually very high. This high voltage can originate arcing, which will produce local melting. Also, the excited species in the plasma are very energetic and bombard the sample with great velocity, generating a great amount of heat. This leads to surface roughening and possible local melting.

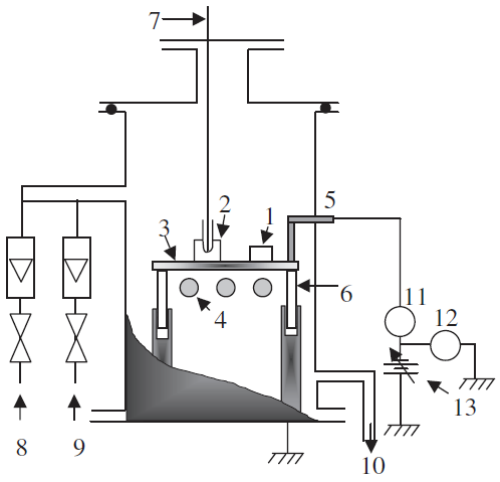

Fig. 5 – Schematic example of DC plasma equipment [7]. 1) sample; 2) dummy sample; 3) table; 4) heater; 5) cathode; 6) insulator; 7) thermocouple; 8)/9) gas inlets; 10) to pump; 11) amp. Meter; 12) Volt meter; 13) DC power supply.

RF Plasma

Fig. 6, shows an example of an RF plasma apparatus. Here there is an inductive coil placed outside the chamber, responsible for plasma generation, a DC between the chamber and the workpiece that has the sole function of accelerating ions. This way the DC bias does not need to be as high, preventing the problems associated with DC plasma but producing very thin layers [5]. The use of hollow cathodes is frequent in this type of setup [8].

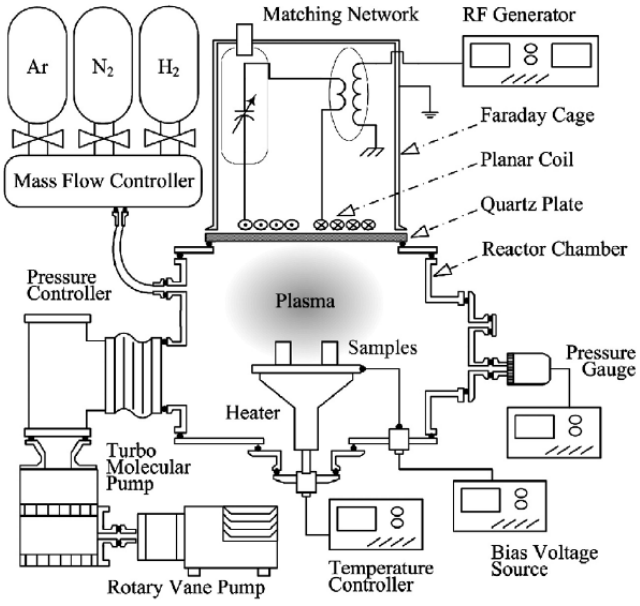

Fig. 6 – Schematic example of radio frequency plasma nitriding equipment [5].

High Density Plasma Nitriding

High Density Plasma Nitriding (HDPN) is the name, given in recent articles, to methods that combine DC and RF plasma generation. By combining these two methods, it is possible to create energy collisions and to confine these collision to a specific region in the chamber. Understanding the magnetic fields involved in the process is essential to understanding this process, though currently there is little knowledge in this regard.

2.4.2. Process parameters

For the purpose of this work let us consider only the process parameters of a high density plasma machine. DC voltage, RF voltage, holding temperature, processing time, gas pressure and gas ratio should change according to composition and geometry of the part to be nitrided.

The influence of the many process parameters in the resulting nitrided workpiece is still trial based and not fully understood. Nonetheless, some conclusions have been drawn [5] [9]:

- Higher gas pressure leads to higher nitrogen activity and density near the surface of the workpiece which, in turns, leads to higher AlN formation rate;
- Nitrogen-hydrogen mixture is the most suitable for nitriding as hydrogen acts as a catalyst, promoting AlN formation. Mixture ratio depends on the aluminum alloy;
- For pure aluminum, at lower treatment times the nitride layer grows linearly in time. After a certain period, as the diffusion of N into the matrix becomes hindered by the newly formed AlN layer, the processing time and the resulting layer thickness have a parabolic dependence, as shown in Fig. 7;

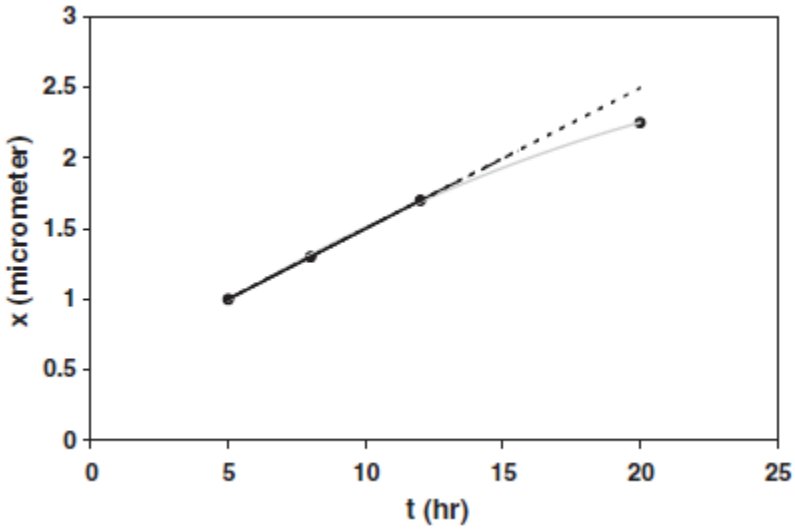

Fig. 7 – Nitride layer thickness has function of nitriding time for Al 1100 [9].

- Surface roughness can be effectively controlled by varying applied DC voltage. Higher voltages produce rougher surfaces due to severe sputtering by ions with high kinetic energy. RF plasma produces smoother surfaces than DC plasma.
- NH radicals contained in the nitrogen-hydrogen plasma have been shown to react with Al_2Cu precipitates in cu-based alloys, acting as catalist for AlN formation [10].

Previous research has demonstrated that surface hardening of Al-Cu alloys is possible by using HDPN equipment [11]. Fig. 8 shows hardness values for a nitrided AA2011 sample between 400 HV and 800 HV, with loads of 50 g (0.5 N) and 10 g (0.1 N), respectively.

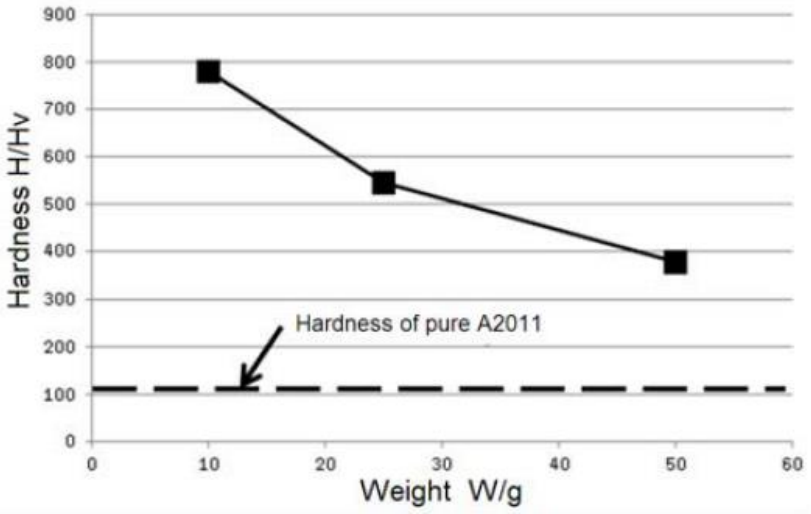

Fig. 8 – Variation of surface hardness with testing load. Sample is AA2011 nitrided with HDPN. [11]

2.5. AlN and its formation

In equilibrium phase, aluminum nitride (AlN) has a hexagonal close packed wurtzite structure, as shown in Fig. 9, with mass density equal to $3.26\ \mathrm{g/cm^3}$. It is thermally stable (melting temperature of $2490\ ^{\circ}\mathrm{C}$ [12]), chemically stable, resistant to corrosion and very resistant to wear (1200 HV [13]). Alongside excellent tribological properties it has other interesting thermal, electrical, optical and acoustic properties. For temperatures of $25\ ^{\circ}\mathrm{C}$ and $600\ ^{\circ}\mathrm{C}$, AlN has a high thermal conductivity coefficient of $30.1\ \mathrm{Wm^{-1}K^{-1}}$ and $20.1\ \mathrm{Wm^{-1}K^{-1}}$, respectively, and small and relatively constant thermal expansion coefficient of $4.84\ \times 10^{-6}\ \mathrm{K^{-1}}$. It has a high specific electrical resistivity of $10^{13}\ \Omega m$, it has piezoelectric properties and it is highly transparent for wavelengths from $200\ nm$ to $12.5\ \mu\mathrm{m}$. Because of all these properties, AlN has a variety of applications in many industries such as tooling, optoelectronics and telecommunications.

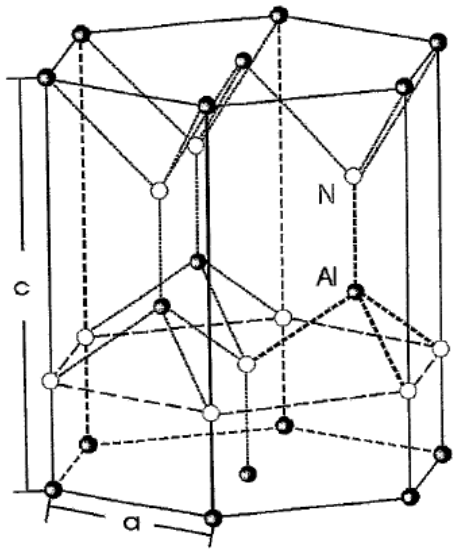

Fig. 9 - AlN wurtzite structure with lattice constants $a = 3.11$ Å and $b = 4.98$ Å [3].

Formation mechanism of the nitride layer by plasma nitriding on an aluminum substrate is illustrated in Fig. 10.

During the pre-sputtering phase, considering the chamber contains only N_2, many excited species form when the gas is ionized. The positive charged species are accelerated towards the cathode and, if the energy is sufficient (this usually happens with the heavier N_2^+ species), the collisions will break the Al_2O_3 layer. The oxide layer will not form again as the chamber has minimum O_2 content. At this stage some AlN may form but the

conditions are not favorable because of the high mobility of the reactive species in the plasma.

In the nitriding phase, the excited nitrogen species either react with the Al atoms on the substrate, or with sputtered Al atoms and then deposit on the substrate. After this the nitrogen atoms migrate away from the surface, into the substrate. and form a layer with a negative concentration gradient, a functionally graded material. This creates very good adhesion and minimizes the problems associated with ceramic coating of metals, like cracking because of different thermal expansion coefficients. After coming into contact with air, AlN reacts with air moisture creating a thin layer of aluminum hydroxide and giving the surface a darker color. The formation rate of $Al(OH_3)$ is very slow and thus it protects AlN from further oxidation.

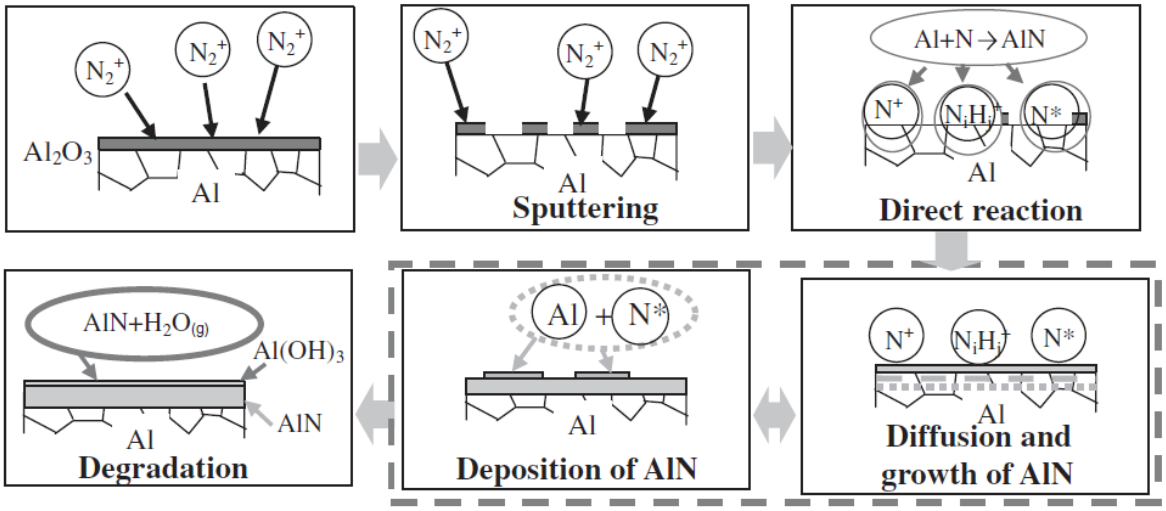

Fig. 10 – AlN formation on the surface of pure aluminum in nitrogen-hydrogen atmosphere [7].

During the nitriding phase, if the AlN formation rate is higher than the diffusion rate of nitrogen into aluminum, a very thick layer with bad substrate adhesion will form. Fick's first law of diffusion gives the diffusive flux in $\mathrm{mol/m^2 s}$ as

$$J = -D\frac{\partial \Phi}{\partial x};$$

where D is the diffusion coeficient in $\mathrm{m^2/s}$, Φ is the concentration in $\mathrm{mol/m^3}$, and x is the length in the direction of diffusion in m. As can be seen the flux decreases as the layer grows because the concentration gradient $\partial\Phi/\partial x$will be progressively less negative. It is possible to control the diffusive flux by controlling the diffusion coefficient D given by

$$D = D_0.e^{-E_A/kT};$$

where D_0 is the maximum diffusion coefficient in m^2/s, E_A is the activation energy in J/mol, k is the Boltzmann constant in J/K and T is the temperature in K.

The diffusion coefficient of nitrogen in pure aluminum has been investigated in [14] and [15], which reported values between 10^{-17} and $10^{-19}\,\mathrm{m}^2/\mathrm{s}$, for temperatures in the range of 500 ℃ to 600 ℃. These coefficients are far lower than those for Iron, which are around 10^{-11} and $10^{-12}\ \mathrm{m}^2/\mathrm{s}$. However, these values refer to nitrogen diffusion in pure aluminum bellow the solubility limit. After a few seconds of nitriding, this limit is surpassed, AlN starts to form and then it is nitrogen diffusing in an Al/AlN matrix. Also, the addition of some alloying elements may have a great effect on diffusion.

2.6. Characterization of Nitrided Surfaces

Nitrided surfaces are characterized by depth of penetration, composition, hardness, roughness and morphology. Depth of penetration is usually measured by direct measurement on a cross section cut; composition is usually determined by X-Ray Diffraction (XRD) [16] or Glow Discharge Spectroscopy (GDS) [9]; hardness is measured by Vickers microindentation tests or Atomic Force Microscope (AFM) [5]; surface morphology is analyzed with SEM; and surface roughness is measured with dry wear tests, such as pin-on-disc [10].

2.7. Summary

In summary, the current research on nitriding of aluminum alloys shows that this technique improves surface properties, though the results reported are still somewhat inconsistent. One of the reasons is that aluminum is more challenging than steel in what concerns diffusion rates. Some alloys, as well as some workpiece geometries, may be more suitable. Advances in plasma technology combined with the ongoing research in this field will certainly bring forth new findings in the near future.

3. ELECTRICAL CHARACTERIZATION

In addition to the characterization techniques mentioned in 2.6, electrical tests may be used to determine the properties of the nitrided layer. In this work, Eddy Currents (EC) testing is proposed as a non-destructive method for determining some of these properties. The NDT lab in FCT has extensive experience in the development of inspection techniques that both EC and 4-point probes. EC tests have been used to describe changes in processed materials, for example, by correlating hardness and electrical conductivity, at various depths, in aluminum alloy FSW joints [17], and for measuring electrical conductivity changes in friction stir surfaced aluminum alloys [18].

3.1. Characterization by Eddy Currents

Eddy currents inspection is a non-destructive technique that relies on the principles of electromagnetic induction to evaluate physical, structural and metallurgical properties of electrically conductive ferromagnetic and nonferromagnetic metal parts. It is used to measure electrical conductivity and magnetic permeability in order to determine alloy composition, microstructure and hardness, and to locate defects such as cracks, voids and inclusions. It can also be used to determine the thickness of non-conductive coatings on conductive substrates or non-magnetic metal coatings on magnetic metal substrates. [19] [20] [21].

Eddy currents testing does not require direct electrical contact with the inspected part and it can be performed at high speeds, therefore it is adequate for inspection in industrial production lines. Because it is based on indirect measurement, the correlation between the instrument readings and the material characteristics must be established beforehand.

In this work, eddy currents testing will be used to correlate the measurements of electrical conductivity and *lift-off* with the characteristics of the nitrided layer.

Fundamentals

An inspection coil is excited by an alternating current (AC) creating a (primary) magnetic field, according to the Biot-Savart law. When the coil approaches a conductive material (Fig. 11), the primary magnetic field (blue) induces a current (red) in the material. According to Lenz's Law, this induced current will create a secondary magnetic field (yellow) contrary to the first.

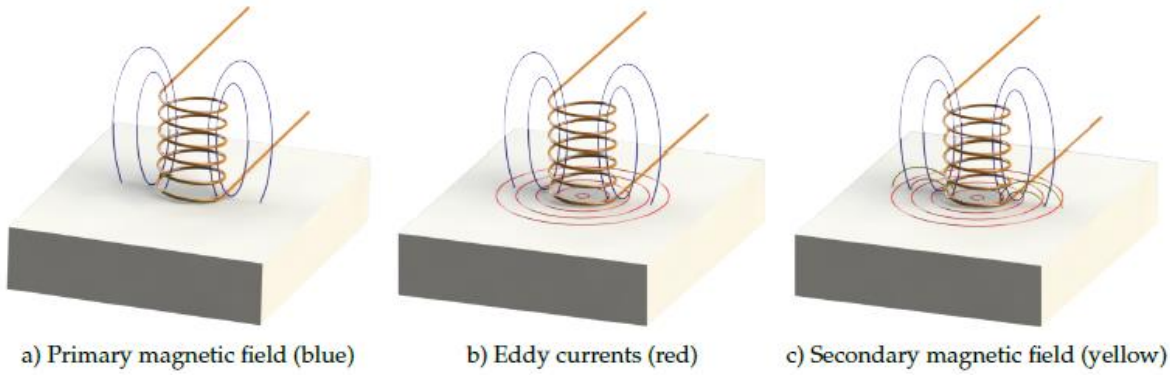

Fig. 11 Electromagnetic induction in eddy currents testing. Primary magnetic field (blue), generated by AC current circulating in the coil, induces an AC current (red) in the inspected part. This current creates a secondary magnetic field (yellow) that opposes the primary field.

Eddy currents testing is based on the impedance variations of the inspection coil as it travels on the surface of the inspected material. These variations are caused by changes in the *lift-off*, in the magnetic permeability of the material (μ) and in its electrical conductivity (σ). These changes are in turn caused by variations on the microstructure of the material, by the presence of defects, or by other factors. Each factor has a characteristic impedance curve, has seen in Fig. 12.

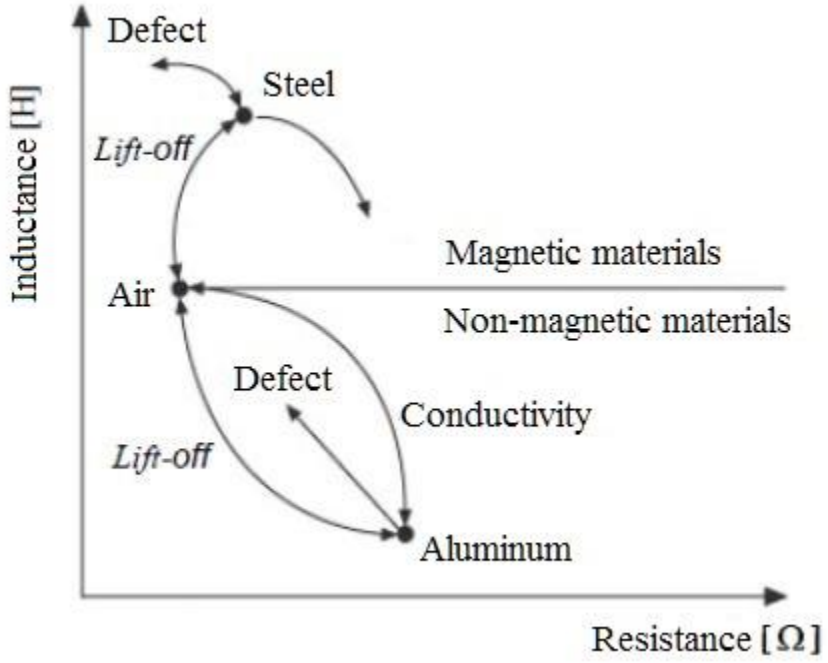

Fig. 12 – Eddy Current impedance response plane [22](adapted)

This technique has low accuracy for higher depths because the density of the eddy currents decreases with depth, in a phenomenon called *skin effect*. In the NDT industry, the consensual limit of penetration is reached when current density is reduced to $e^{-1} \approx 36.78\ \%$ of its surface value. Dept of penetration δ is given by

$$\delta = \frac{1}{\sqrt{\pi f \sigma \mu}}$$

where f [Hz]is the frequency of the alternating current in the exciting coil, σ $[\mathrm{S/m}]$ is the electrical conductivity and μ $[\mathrm{H/m}]$ is the magnetic permeability of the material. For a given material, inspection depth can be controlled by adjusting the frequency of excitation. Electrical conductivity and magnetic permeability of the material are thus the limiting factors of eddy current penetration.

In conclusion the EC currents technique is a widespread method for non-destructive testing in the industry. Lately, with the development of new variants and new probes, this method has been applied in the characterization of metal matrix composites (MMC) and Functionally Graded Materials (FGM) modified by FSP and other processes. Here it is used experimentally in this developing diffusion heat treatment.

4. EXPERIMENTAL PROCEDURE

4.1. Materials

For this study AA2011 samples with 0.4% Si, 0.7% Fe, 5.0-6.0% Cu, 0.2-0.6% Bi, 0.2-0.6% Pb, 0.3% Zn, and 0.05% Ti were used. Electrical resistivity (μ) of this alloy is around $45x10^{-9}\ \Omega.\mathrm{m}$ which corresponds to a conductivity of circa 39% IACS.

The samples were cut from a mechanically alloyed rod with 0.2 x 5 mm diameter with two different types of finishing: polished with diamond past to a mirror like-surface with sharp, as-cut edges (Type 0) and polished with sandpaper, beveled edges (Type 1) and with an orifice on the back surface to attach the thermocouple (Fig. 13).

a) 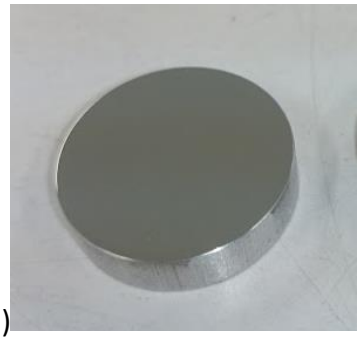 b) 

Fig. 13 – a) Type 0 sample mirror like-surface with sharp, as-cut edges; b) Type 1 sample polished with sandpaper and beveled edges

Prior to the introduction in the vacuum chamber, samples were cleaned with ethanol to remove any contaminants. Once inside the chamber, electrical contact between the samples' surface and the base plate was always checked using a multimeter, before starting the process. Because the base plate is made of steel, it also gets nitrided and therefore electrical contact may be hindered.

4.2. Nitriding Equipment

A YS Denshi nitriding machine, illustrated in Fig. 14, was used to produce samples. This is a complete plasma nitriding and ashing system specially designed for surface nitriding of steel parts, though it is also used experimentally for aluminum alloys.

It comprises a water cooled steel vacuum chamber (1), a vacuum system with a primary and a secondary pump (2), a $250\ \mathrm{W}$ RF dipole power supply (3), a $600\ \mathrm{V}$ DC bias power supply (4), a PLC controller with a control panel (5), a water cooling system(6), a gas feed system(7) and a general power supply unit (8).

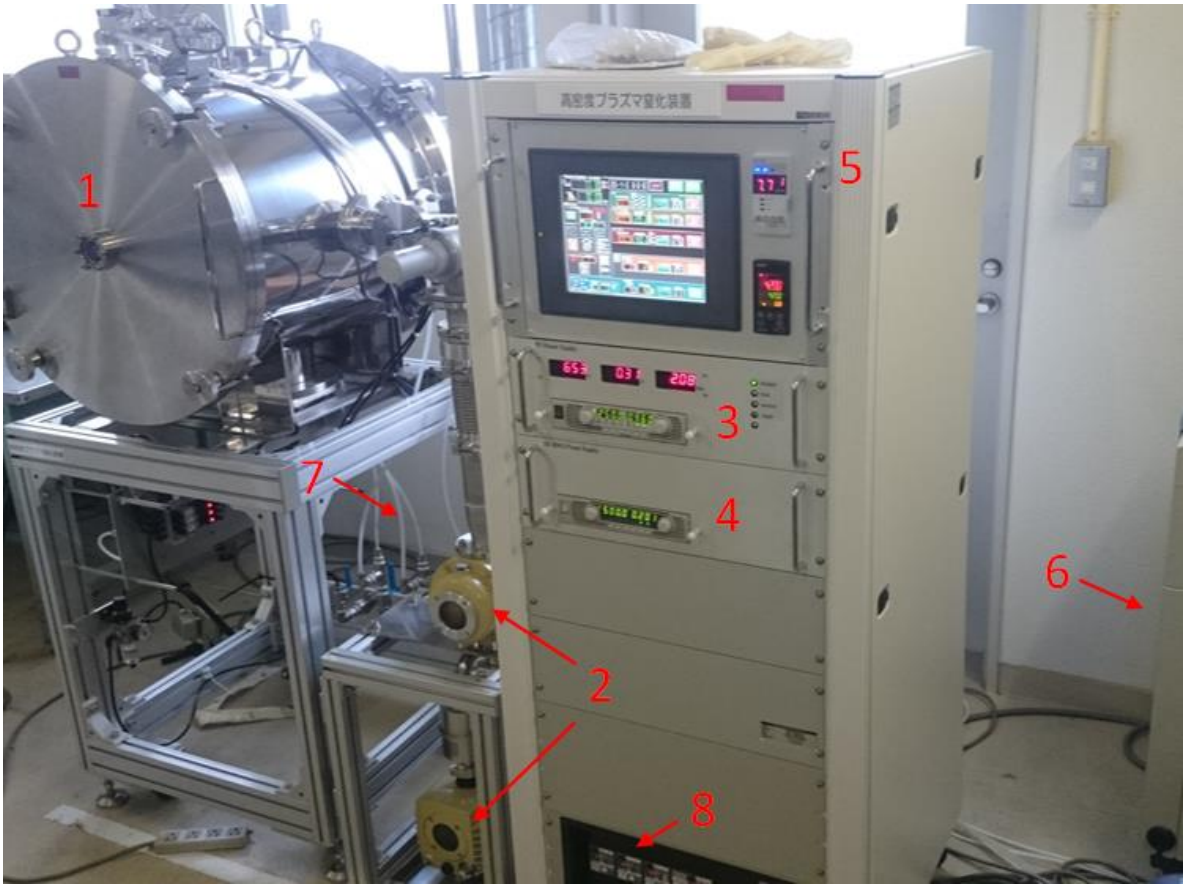

Fig. 14 – Nitriding equipment: 1) vacuum chamber; 2) vacuum pumps; 3) RF power supply; 4) DC bias power supply; 5) PLC controller; 6) cooling unit; 7) gas feed lines; 8) power unit.

The control panel allows the setup of pressure (>0.1 MPa), DC bias voltage (0-600 V), RF voltage (60-250 V), N_2 and H_2 flow rates, each one independently from 20 to $1000\ \mathrm{ml/min}$; and heating temperature up to $550\ ℃$. It also shows real time readings of each parameter.

The interior of the vacuum chamber, shown in Fig. 15, is composed of 1) two RF electrodes, 2) a thermocouple, 3) a heater plate and 4) a gas feed. The RF electrodes and the heater plate are supported by ceramic bushings to keep them at a different electrical potential than the chamber. The heater plate has a planar coil on the inside, to generate heat by Joule effect and it is also where DC bias is applied. The gas feed tube, not pictured here, is a 30 cm flexible steel hose.

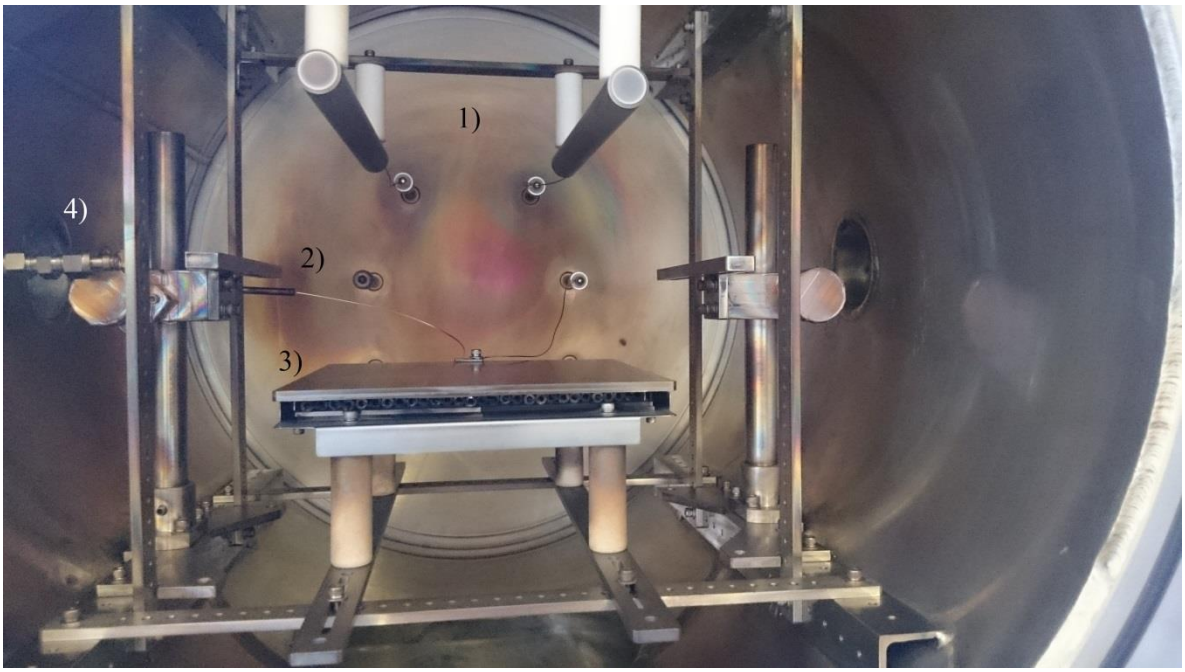

Fig. 15 – Interior of the vacuum chamber. 1) RF electrodes, 2) thermocouple, 3) heater plate and 4) gas feed (tube not pictured).

4.3. Parameters

To establish a starting point, a set of samples was processed using parameters of a previous work [11]. The cathode configuration used in this work is not reported, though a hollow cathode is mentioned. The experiments were divided into two groups, based on the processing temperature T: in the first group T was $400℃$ was used on all experiments, while in the second group all experiments were done bellow $200℃$. Processing parameters of the first group, from here on out referred to as *hot processed*, are show in shown in Tab. 1.

Tab. 1 – Sputtering and nitriding parameters of *hot processed* samples.

Hot samples		**DC (V)**	**RF (V)**	**P (Pa**	**T (℃)**	**Duration (s)**	N_2 $(\mathbf{ml/min})$	H_2 $(\mathbf{ml/min})$	**Cathode config.**	**Sample type**
H1	Sputt.	500	0	70	420	1800	150	0	e)	0
	Nitr.	500	250	70	420	14400	150	23		
H2	Sputt.						150	0	a)	
	Nitr.					1800	150	23		
H3	Sputt.	350	0	30	400	1800	80	0	c)	0
	Nitr.	350	250	75	400	14400	80	20		
H91, H92, H93	Sputt.	350	0	75	400	1800	80	0	e)	0(covered with a thin steel disc)
	Nitr.	350	250	75	400	14400	80	20		

For the second group lower temperatures were selected since, in the first group, a sharp drop in hardness of non-treated material was observed. This was due to tension relief from the cold work. Also, temperatures in this range are important for future applications to avoid annealing in heat-treated parts. Parameters used in the second group of experiments, from this point forward referred to as *cold processed*, are shown in Tab. 2.

Tab. 2 – Nitriding parameters *cold processed* samples.

Cold samples	**Heating (℃; s)**	**DC (V)**	**RF (V)**	**P (Pa)**	**Duration (s)**	**Cathode configuration**	**Sample type**
H6	100;1200	400	250	70	3600	a)	0
C3; C31; C32	86;1200	300	250	70	3600;10800;10800	a)	
C41, C42,C43,	35;150	300	250	70	14400	b)	1
C45; C46;	85;600s	300;470			18000		
C47; C48, C49	200;1260s	470			18000		
C5, C51; C52	86; 1200s	300; 400; 470	250	70	14400	b)	1(covered with a half thick disc)
T1;	86;150s	300	250	70	10800	c)	1
T11; T12; T13; T14	35;150s	470					
T2; T21	35; 150s	300				d)	
B1	100;1200	470	250	70	10800	c)	1
B2	150;1200				14400		
B3	180;1200 (always on)						
B31	180;1200 (always on)	450	250	70	18000	c)	1
B33	180;1200 (always on)	460					
A1, A2	100;1200	470	250	70	10800	e)	1
A3	150;1200				14400		
A4	180;1200				14400		

The following heating procedure was used for most samples: after evacuation, nitrogen was introduced until a pressure of around $300\ \mathrm{Pa}$ was reached; the heater was turned on for a specified amount of time, set to the desired nitriding temperature; the chamber was re-evacuated and refilled to $70\ \mathrm{Pa}$; and finally the pre-sputtering was started. In some experiments the temperature measurements of the thermocouple were registered.

After having some understanding of how the plasma behaves, some modifications were made to the previous cathode configurations and new configurations were tested.

Sputtering of the *cold processed* samples was done at $70\ \mathrm{Pa}$ for $1800\ \mathrm{s}$ with $470\ \mathrm{V}$ DC (no RF), with a gas flow of $80\ \mathrm{ml/min}$ of N_2 (no H_2). Sample H6 was sputtered with $400\ \mathrm{V}$ DC, with all other parameters equal.

A ratio of 4:1 of $N_2$to H_2 was used for nitriding in all experiments. Previous research has reported maximum hardness values of around $900\ \mathrm{HV}$ with this ratio [11]. Therefore, following the references as a starting point, N_2 flow rate was set at $80\ \mathrm{ml/min}$ and H_2 to $20\ \mathrm{ml/min}$.

Research also shows that the gas content, along with other parameters, has a significant effect on the final result, since it determines which excited species are present in the plasma. This parameter requires further study to be fully understood but this is out of the scope of this thesis.

After placing the samples in the vacuum chamber pumping was carried out until the pressure reached around $0{,}7\ \mathrm{Pa}$. Nitrogen gas was introduced to a pressure of around $300\ \mathrm{Pa}$ and pre-heating was performed, according to Tab. 1 and Tab. 2. After pre-heating, the chamber was evacuated again to minimize contamination. Finally, it was refilled with nitrogen at the specified pressure for each sample and pre-sputtering was initiated. About $30s$ before the end of the established sputtering time, hydrogen feed was started. Nitriding was initiated has soon as sputtering ended.

4.3.1. Cathode Configurations

To assess the effects of cathode geometry, the cathode configurations shown in Fig. 16 were used. The position of the gas feed tube was also taken into account.

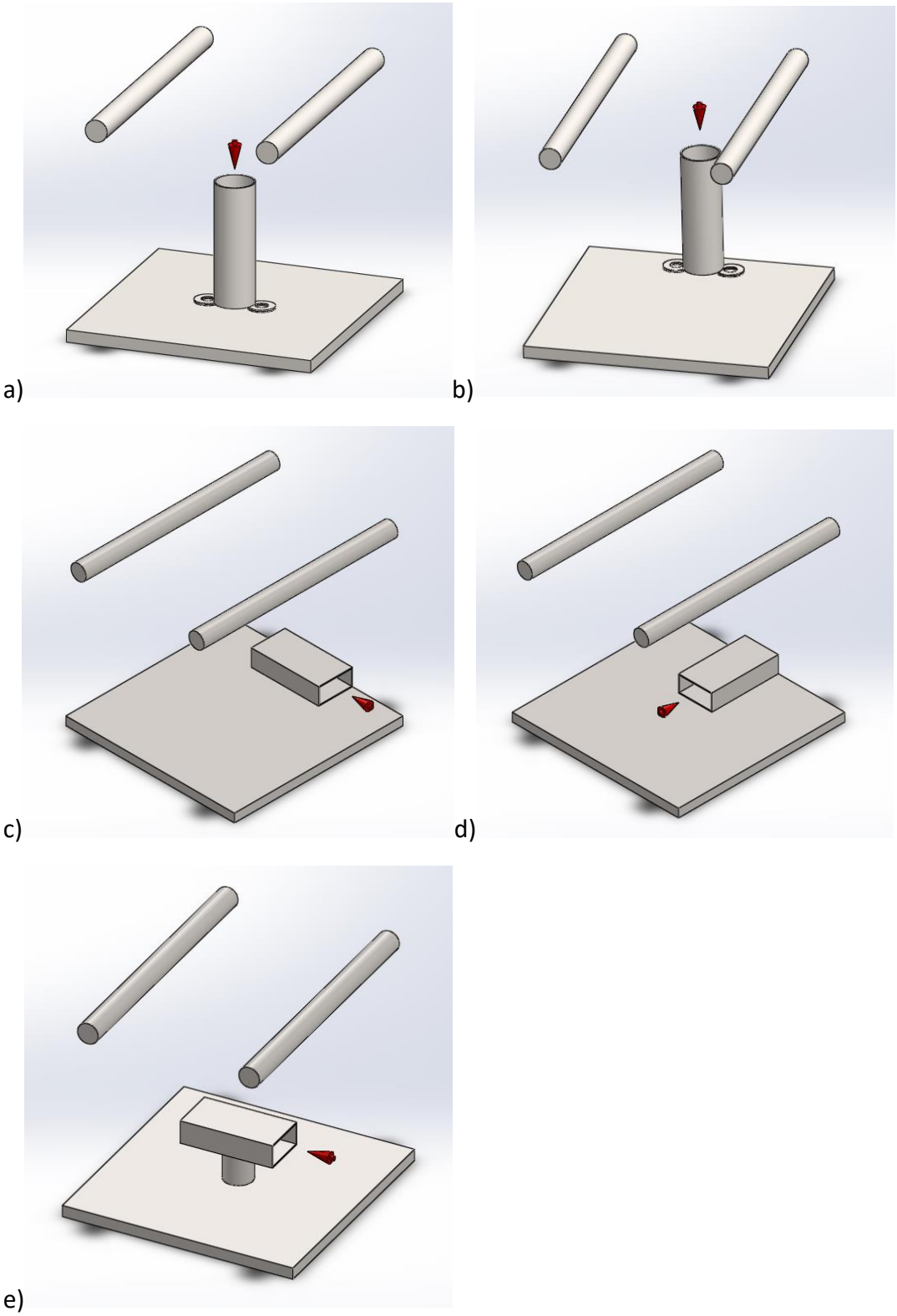

Fig. 16 – Cathode configurations used in *hot* and *cold processed* experiments. Samples placed on the inside of the hollow tube. Red arrow indicates the position of the gas feed tube.

4.3.2. Cover for Electrical Conductivity Tests

Some samples were partially covered in order to obtain a nitrided area, as well as a non nitrided area on the top surface. This way a direct comparison can be done between treated and untreated surfaces.

Samples H91 to H93 were covered with a thin steel disc placed in the center (Fig. 17a) while C5 to C52 were covered with a thick aluminum half disc (Fig. 17b). Samples C41 to C49 were covered, like in Fig. 17b, with Kapton tape, which later proved to be inefficient since it has around 21% of oxygen in its composition.

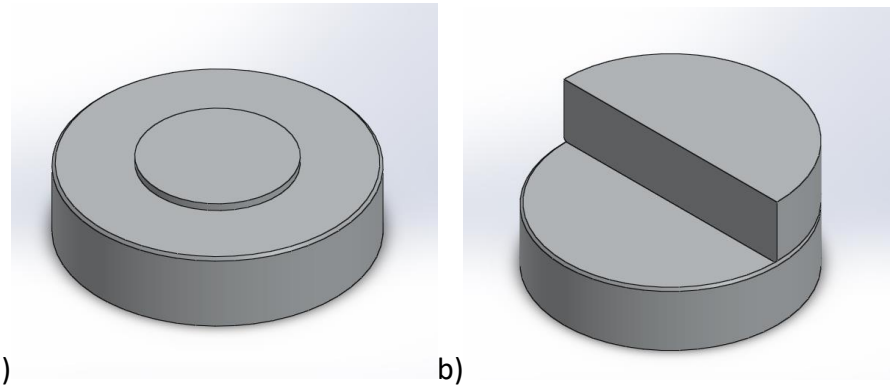

a) b)

Fig. 17 –Samples covered with a) a thin steel disc and b) a thick aluminum disc, to obtain an non nitrided area for reference during the electrical conductivity measurements.

4.3.3. Temperature Measurements

Experiments T1, T11, T12, T13, T14, T2, and T21, were conducted in order to study the temperatures generated with cathode configurations c) and d). For this purpose the thermocouple was placed in different locations: on the heater plate (T11, T12 and T21), on the top surface of the sample (T1 and T2, Fig. 18a) and on the back of the sample, outside the hollow cathode (T13 and T14, Fig. 18b).

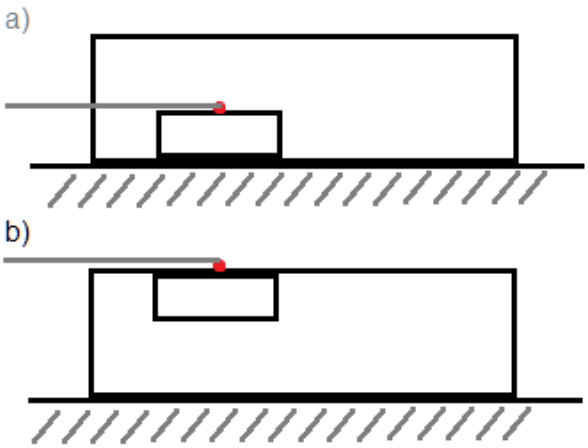

Fig. 18 – a) Location of thermocouple for sample T1 and T2; b)location of thermocouple for samples T13 and T14

4.4. Testing

As the samples were processed, some tests were performed to determine the homogeneity of the nitride layer, its conductivity and its hardness. Initially, as soon as the specimens were removed from the vacuum chamber they were visually inspected to assess the color of the surface and its uniformity. After this the surface was inspected with the optical microscope, multimeter and SEM in order to have a qualitative overview of the result. For quantitative measurements, Vickers microindentation tests and EC tests were performed. The possibility to correlate the surface properties and the electrical conductivity data was investigated.

4.4.1. SEM

The nitrided samples were tested by Scanning Electron Microscopy with a JEOL JCM-6000 Benchtop SEM, to analyze the surface structure and morphology.

4.4.2. Electrical conductivity

Electrical conductivity tests, namely EC tests, were performed at the NDT lab in DEMI, FCT-UNL. The equipment used incorporates a customized EC probe, an in-house developed positioning system (Fig. 19) and a data acquisition computer.

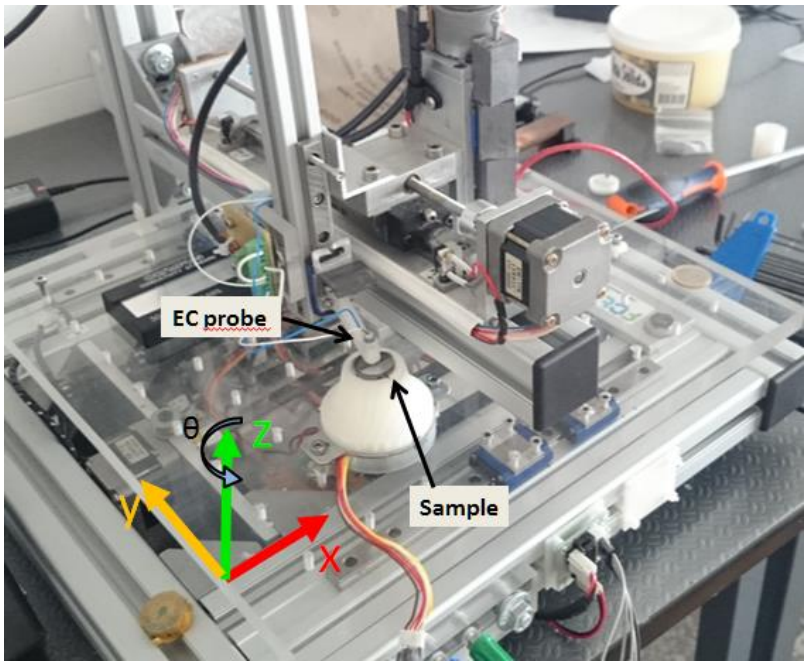

Fig. 19 – Eddy currents test positioning system.

The positioning system is able to work with both Cartesian and polar coordinates. In this specific case, polar coordinates were used in order to have faster swiping tests, taking full advantage of the available area while avoiding the edges of the specimens. A support base, designed in SolidWorks and printed using the 3D printer at the NDT lab, was used to place the samples on the rotating base, ensuring correct positioning during the tests.

The EC probe is a helical cylindrical type probe with over 100 turns and a ferrite core. It is appropriate for use in a range of frequencies between $100\ \mathrm{kHz}$ and $1\ \mathrm{MHz}$. For this range, the depths of EC penetration in AA2011 are shown in Tab. 3.

Tab. 3 – Eddy current penetration depth of each AC current frequency

	$f_1 = 100\ \mathbf{kHz}$	$f_2 = 500\ \mathbf{kHz}$	$f_3 = 1\ \mathbf{MHz}$
Penetration depth $\delta\ [\mathbf{mm}]$	0.334	0.149	0.106

The EC tests were performed in clockwise swipes with the two resolutions shown in Tab. 4. The swiping area is comprised between $r = 1\ \mathrm{mm}$ and $r = 9\ \mathrm{mm}$, avoiding the effect of the center hole in the type 1 samples and the edge effect. For each specimen and for each frequency, two tests were performed: one to measure conductivity and one to measure *lift-off*. The results were plotted in 3D graphs and analyzed.

Tab. 4 – Resolution of EC tests.

	Radial steps $Res_\rho(\mathbf{mm})$	Angular increments Res_θ
Res.1	0.25	3.6°
Res.2	0.08	0.9°

4.4.3. Hardness measurements

Vickers hardness tests were performed using an Akashi MVK-H1 hardness tester. Loading time was $15\ \mathrm{s}$ for all samples. The applied loads varied from $10\ \mathrm{gf}$ to $200\ \mathrm{gf}$, or $0.098\ \mathrm{N}$ to $1.96\ \mathrm{N}$. This equipment has an integrated microscope and measuring system.

5. RESULTS AND DISCUSSIONS

In this chapter the processed samples and the temperature measurements are analyzed and discussed. Results of the electrical conductivity and mechanical tests are presented and interpreted.

5.1. Process tuning

Prior to obtaining satisfactory nitrided results, many experiments were conducted. Initially the parameters reported in the literature were used, to which some adjustments were made in what concerns DC bias, temperature and hollow cathode configurations. Other parameters like gas content, pressure and RF voltage were kept constant for all or most of the experiments. The following results are the product of iterative tuning of the nitriding process.

5.1.1. Hot processed samples

Starting with the parameters reported in [11], the result obtained was a very dark and smooth sample as seen in Fig. 20.

a)  b) 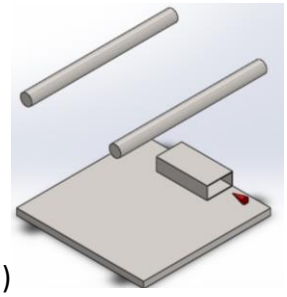

Fig. 20 – Sample H3 after processing (a) and respective cathode configuration (b).

Hardness tests of the nitrided layer were inconclusive because small loads did not produce visible indentations, suggesting an increased hardness on the surface, but, higher loads produced indentations with very distorted contours, indicating the layer was penetrated through. Vickers tests of the back of the sample revealed a decreased in hardness of the non nitrided aluminum, associated with stress relief from the heat treatment. The hardness results of $800\ \mathrm{HV}$, reported in [11], were impossible to verify.

Next, the DC bias was increased from 350 V to 500 V and tested with cathode configurations a) and c). As shown in Fig. 21, the result was excessive deposition in both cases. With configuration a) the deposited layer is around $0.5\ \mathrm{mm}$, it is cracked and completely detached from the substrate in some places. With configuration c) the layer is much thinner but still has adhesion problems on the edges. It is clear that AlN formation is not a problem but good adhesion of the layer is.

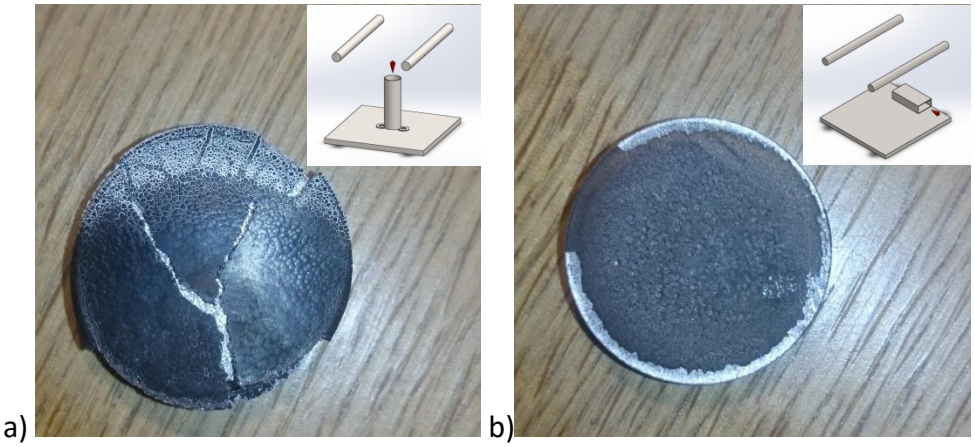

Fig. 21 – Samples a)H1, nitrided with cathode configuration a); and b)H2, nitrided with cathode configuration c). Both exhibit excessive nitride deposition and severe delamination.

The DC bias was lowered again to 350 V but this time, the specimen was covered with a thin metal disc. Also, cathode configuration e) was used, which means the hollow cathode was placed in an elevated position. Fig. 22 shows the results obtained in three consecutive experiments. The samples have an increasingly lighter color which may be caused by changes in the conductivity of the cathode. The color of each one is also not very homogeneous. It seems the disc has an effect on the surrounding area, hence the heterogeneous but axisymmetric aspect of the surfaces.

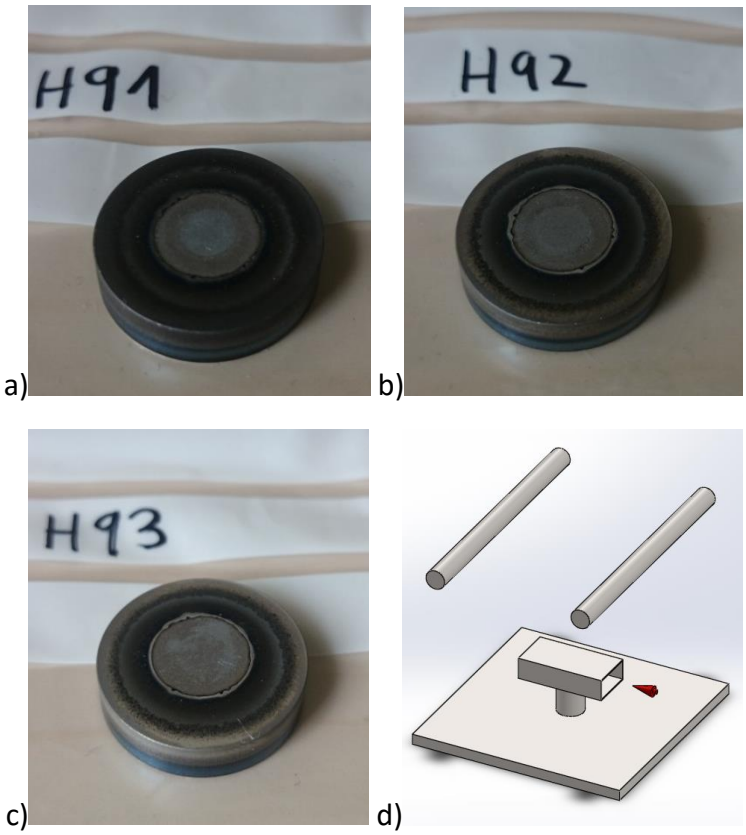

Fig. 22 – Samples H91, H92 and H93 after processing (a, b and c) and respective cathode configuration (d).

The *hot processed* samples show promising results in terms of nitride layer formation but the samples showed a decrease in hardness of the substrate. This is due to stress relief, however, a heat treatment at temperatures from 250 ℃ to 400 ℃, for these processing times, will anneal every Al-Cu alloy. From an industrial view point it is important to have a nitriding process that can be applied to finished components (tempered, aged, etc.), hence the *cold processed* experiments were performed.

5.1.2. Cold processed samples

The objective with these experiments was to achieve good nitrided layers with processing temperatures considerably lower than the ones reported in previous articles [4] [5] [9] [11]. Lowering the temperature means N diffusion in the matrix will be hindered but, AlN formation rate will not be affected because it is fruit of an exothermic reaction [23].

These experiments will also help to understand how much heat is supplied to the workpiece by the plasma and by the nitride formation reactions.

It was immediately clear with the first experiments that the process parameters would have to be tuned in order to achieve results similar to the *hot processed.* Fig. 23 shows the result of the first experiment that exhibited a well visible layer. There was some delamination just by handling the sample, which is a clear sign of excessive deposition. The black color on the edges indicates that these were preferential sites for deposition.

a)  b) 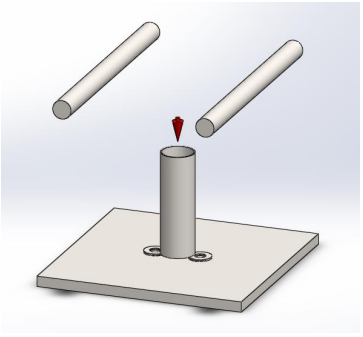

Fig. 23 –a) Sample H6 after nitriding at 100 ℃ for 3600 s(1 h) and b) respective cathode configuration (narrow cylinder).

The cylindrical hollow cathode was replaced by a wider one in order to have more spacing between the edges of the specimen and the inner walls of the cylinder; the specimen was placed higher inside the hollow cathode, to avoid the disturbance in the plasma near the base of the tube; and the DC bias was lowered from 400 V to 300 V. These modifications should improve the gas/plasma flow around the sample and reduce the deposition rate.

As can be seen in Fig. 24 the result obtained is quite interesting, since the sample is only nitrided on the bottom edges.

a)  b) 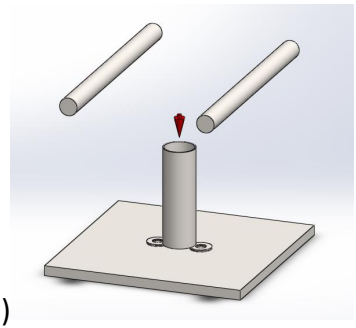

Fig. 24 – a) Sample C3 after nitriding at around 100 ℃ for 3600 s(1 h); b) respective cathode configuration (wide cylinder).

Nitriding for 3 h, instead of 1 h, only resulted in a slight loss in mirror finish on the top surface, as shown in Fig. 25. When observed from the top window of the vacuum chamber, the specimen inside the hollow cathode seemed to be above the high density plasma region. This may have been the reason why only the bottom edges were nitrided.

Fig. 25 – Sample C31 after nitriding at around 100 ℃ for 10800 s(3 h).

Moving the specimen into the middle of the high density region lead to a very uniform color of the nitrided layer. This can be seen in Fig. 26, were the sample has a dark grey color, on the top surface and on the edges, and no delamination. This result is similar to those of the *hot processed* experiments, which suggests that the process is feasible at lower temperatures.

Fig. 26 -Sample C32 after nitriding for 10800 s(3 h), at 300 V, starting at 86 ℃.

Next, the effect of the beveled edges was tested. Using cathode configuration a) the result was a light grey colored surface with slightly darker edges, after 5 h of nitriding (Fig. 27). This suggests that the less sharp edges may be unfavorable in the formation of the nitrided layer.

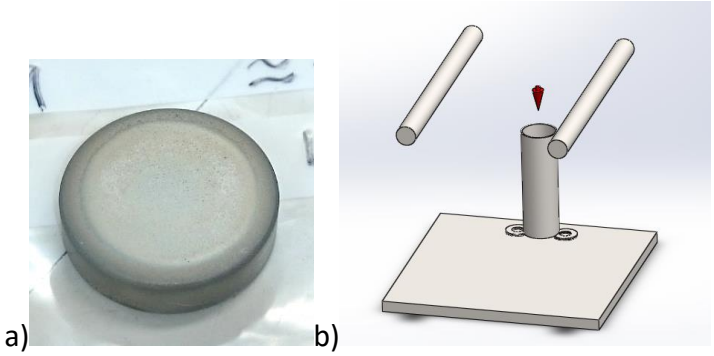

Fig. 27 - Sample C49 after nitriding for 18000 s (5 h) at 470 V, starting at 196 ℃, without heating during the process; respective cathode configuration.

By covering the specimens, as shown in Fig. 28d), the effect of surface geometry was further investigated. The color of the nitrided surfaces gets darker as DC bias increases,

but it is not uniform. The quality of the layer seems to be highly dependent on the geometry of the workpiece.

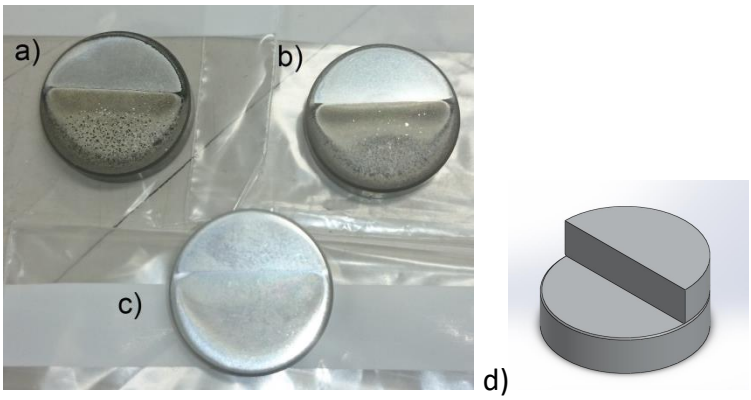

Fig. 28 – a) C51 with 470 V DC bias; b) C52 with 400 V DC bias; c) C5 with 300 V DC bias. All nitrided for 14400 s(4 h), starting at 86 ℃, without heating during the process.

Changing to cathode configuration c) lead to more satisfactory results, as can be seen in Fig. 29. After 4 h of nitriding, starting the process at 150 ℃, the surface was still darker on the edge and it had some nitride clusters. Raising the process temperature to a constant 180 ℃, lead to a uniform, dark grey, though there were even more nitride clusters on the surface that increased its roughness significantly. It should be noted that the processing temperature was the only parameter that changed. The differences seen in Fig. 29 were either caused by the difference in temperature or by other unmeasured factor (e.g. electrical contact between cathode parts, position of sample, etc.).

Fig. 29 – Samples B2 and B3 after nitriding for 14400 s (4 h), at 470 V, starting at 150 ℃ and 180 ℃, respectively.

In an attempt to avoid the nitride clusters by lowering the deposition rate, DC bias was lowered. Fig. 30 shows the results obtained by nitriding with 450 V and 460 V, with cathode configuration c) at a constant temperature of 180 ℃. The nitride clusters were

successfully avoided but the color of the surface, especially on the edges, is much lighter, indicating a thinner coating. Longer processing times may produce better results.

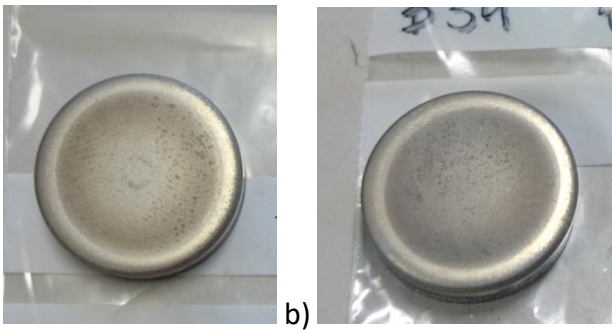

Fig. 30 – a) sample B31 (450 V DC bias); b) sample B34 (460 V DC bias); both nitrided for 18000 s (5 h) at 180 ℃.

All beveled samples exhibit some nitride clusters on the top surface when nitrided with cathode configuration c), therefore, a small change was made. The hollow cathode was moved to the center of the heater plate and placed on top of a steel cylinder. The objective was to find a location where the plasma field is more uniform. This is the configuration seen in Fig. 16e).

The result of this experiment is shown in Fig. 31b). There seems to be a uniform distribution of the layer but the color is very light.

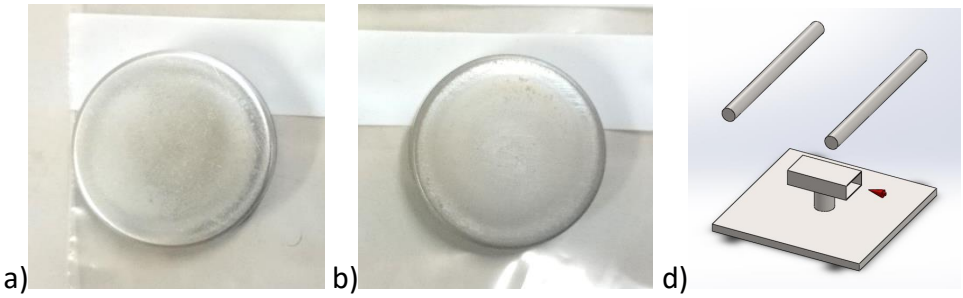

Fig. 31 – Samples a)A1, placed at the entrance of the hollow cathode; and b)A2, placed $3/4$ length inside the hollow cathode. Both pre-heated to 100 ℃ and nitrided with 470 V DC for 10800 s (3 h). d) Cathode configuration used in these experiments.

Another experiment was done with the same parameters but placing the sample at the entrance of the hollow cathode (gas feed side). The result, shown in Fig. 31a), was a slight loss in mirror finish and no evident signs of nitriding. This indicates that this type of hollow cathode has a narrow range of options for sample placement. In this work, the best results were achieved by placing the specimens at about ¾ of the length of the tube.

To improve upon these results, the nitride layer should be made thicker while maintaining the good homogeneity seen in Fig. 31b). For this purpose the temperature was increased to 150 ℃, and then 180 ℃, as well as the processing time, from 3 h to 4 h. Fig. 32 shows the results obtained.

a)  b) 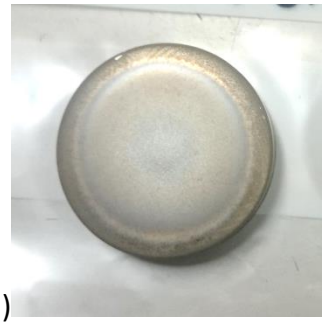

Fig. 32 – Samples a)A3, pre-heated to 150℃; and b)A4, constant temperature of 180℃. Both nitrided with 470 V DC, for 14400s (4h) and with cathode configuration e)

Both results present a dark color, though with some reflectiveness, and a good distribution of the layer. At 180 ℃ the edges seem to have been more nitrided than the center. Incresing the processing time further, maintaining this temperature, might have provided better results. The AlN clusters seen previously are not present here. Configuration e) seems to be the most adequate for these experiments.

5.2. Effects of cathode configuration and DC bias on temperature

Processing temperatures measured with cathode configurations a) and b) are plotted in Fig. 33. These were taken in two experiments that started at different temperatures, one at 200 ℃ (C49) and the other at 86 ℃ (C32).

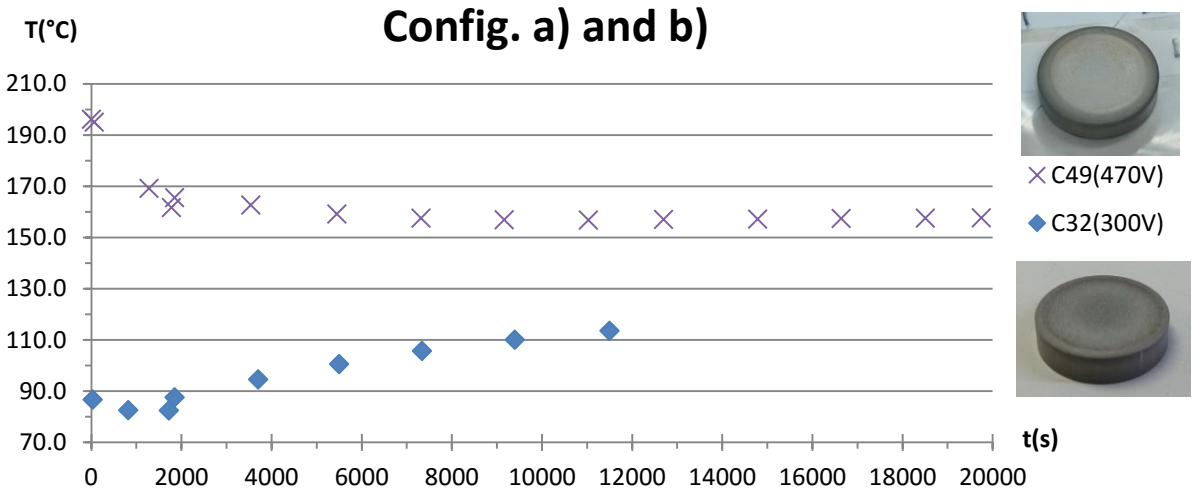

Fig. 33 – Temperature measurements of samples C32, nitride with cathode config a), and C32, nitrided with cathode config. b). Thermocouple on the heater plate.

Since during the pre-sputtering phase both temperatures decreased and, during the nitriding phase C49 maintained a relatively high temperature and C32 increased its temperature, it is safe to assume that a considerable amount of heat is supplied to the cathode during the second phase. The source of this heat must be the high density plasma created inside the hollow cathode due to the strong magnetic field.

It is interesting to see that sample C32, at a much lower temperature and with lower DC bias, seems to be darker in color and more homogeneous than C49, indicating that workpiece geometry (sharp vs beveled edges) and surface roughness may be relevant factors for layer formation.

The temperatures measured with configuration c), namely of samples B1, B2 and B3, are plotted in Fig. 34. Sample B1 increased temperature during the entire process, from $100℃$ to $160℃$, with a tendency to stabilize at the end. B2 started at $150℃$, decreased to $140℃$ during pre-sputtering and increased during nitriding to a stable $165℃$. B3 was made at constant temperature, with only minor oscillations.

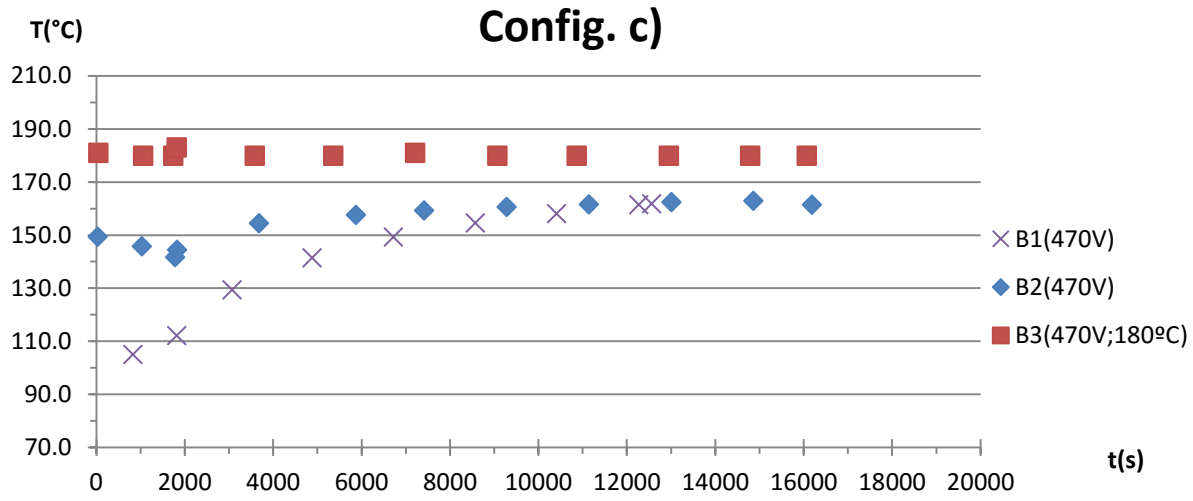

Fig. 34 – Temperature measurements of samples B1 (pre-heated to 100 ℃), B2 (pre-heated to 150 ℃) and B3 (heated to 180 ℃ throughout). All nitride with cathode config c) and 470 V DC bias. Thermocouple on the heater plate.

Fig. 35 shows the temperature measurements done on samples A2, A3 and A4 using configuration e). Every parameter, except for cathode configuration, is the same as in the B samples (A1 analogous to B1, A2 analogous to B2, etc.) so configurations c) and e) can be compared directly.

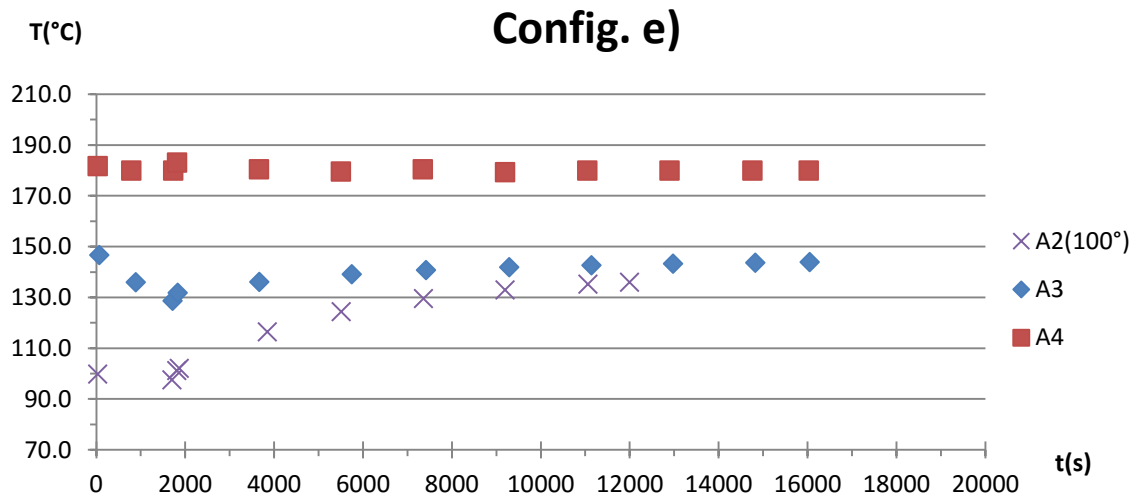

Fig. 35 - Temperature measurements of samples A2 (pre-heated to 100 ℃), A3 (pre-heated to 150 ℃) and A4 (heated to 180 ℃ throughout). All nitride with cathode config e) and 470 V DC bias. Thermocouple on the heater plate.

As can be seen the temperatures follow the same tendencies though, for A2 and A3, the maximum temperatures registered are lower than those of B1 and B2. This may be because configuration e) takes longer to reach thermal equilibrium in all the cathode pieces, since the hollow cathode is further away from the heater plate.

Temperatures measured with cathode configuration c) and d), are plotted together in Fig. 36. As can be seen, starting the process at a temperature of around $35\,℃$, both configurations achieve similar maximum temperatures bellow $170\,℃$. Configuration c) has an increasing heating rate until around 1 h 30 min of starting the pre-sputtering (5400 s), after which it decreases to a steady value until the end of the process. Configuration d) has a very high heating rate on the first seconds of pre-sputtering but, after around 1000 s of processing, the heating rate decreases to a steady value similar to that of c).Towards the end, the temperature of configuration c) surpasses that of d), hinting that the former might achieve higher temperatures for longer processing times.

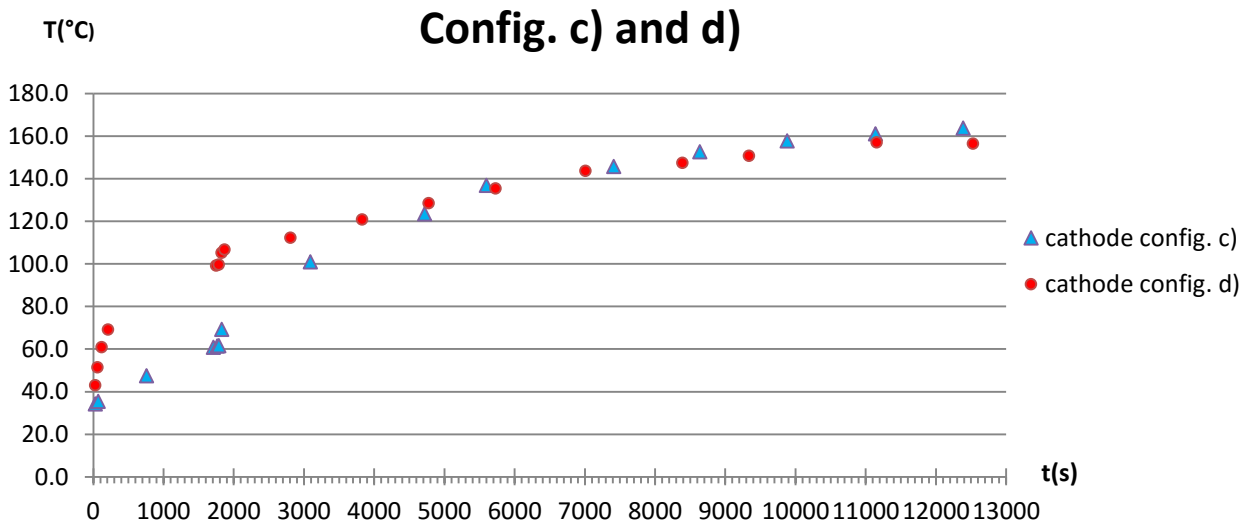

Fig. 36 – Temperatures measured on the heater plate, using c) and d) cathode configurations with 300 V DC bias(samples T1 and T21, respectively)

These experiments were performed with pre-heating only, hence, it should be noted that a considerable amount of heat is supplied by the plasma since the temperatures achieved in both are just below those seen in Fig. 34.

Temperature on the surface of the sample

The temperatures measured at the surface of the sample, for cathode configurations c) and d), are plotted in Fig. 37.

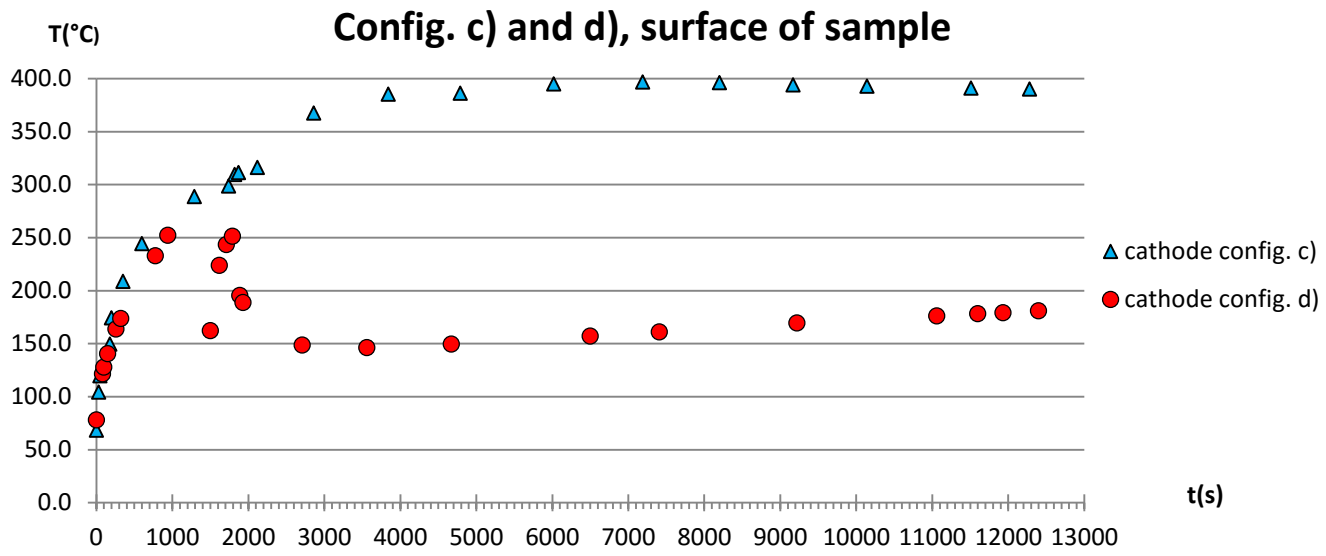

Fig. 37 – Temperatures measured at the surface of the sample with longitudinal (L) and transverse (T) hollow cathode configurations at 300 V DC bias.

During most of the pre-sputtering, both the longitudinal and the transverse configurations show the same temperatures. As soon as the hydrogen is introduced ($1770\ s$), the temperature c) starts to decrease, with some oscilations, while the temperature of d) continues to increase. When the RF is turned on ($1800\ s$), the temperature of c) suffers a considerable decrease, after which the rate of increase is low; and the longitudinal sample continues to increase slowly until it stabilizes at $6000\ s$, just below $400\ ℃$.

During pre-sputtering, because only the DC bias is on, the plasma has the same behavior in both cathode configurations. When the RF is turned on, magnetic fields and eddy currents are generated inside the chamber and in the hollow cathode. Each cathode configuration interacts differently with the generated magnetic field, hence the difference in measured temperatures.

The transverse configuration presents the lowest average temperatures on the surface of the sample in spite of the higher temperature during the pre-sputtering phase. However, since this measurement was taken with the thermocouple wire in the middle of the high density plasma region, it may be inaccurate. Additional experiments are necessary.

Analyzing Fig. 38, it can be seen that this temperature peak at the surface of the sample is not detected when measuring on the heater plate, which may indicate that it is a localized temperature spike that does not affect the substrate. The temperatures plotted are for processes with different DC bias voltages, therefore only the gradients can be compared, not the temperature values.

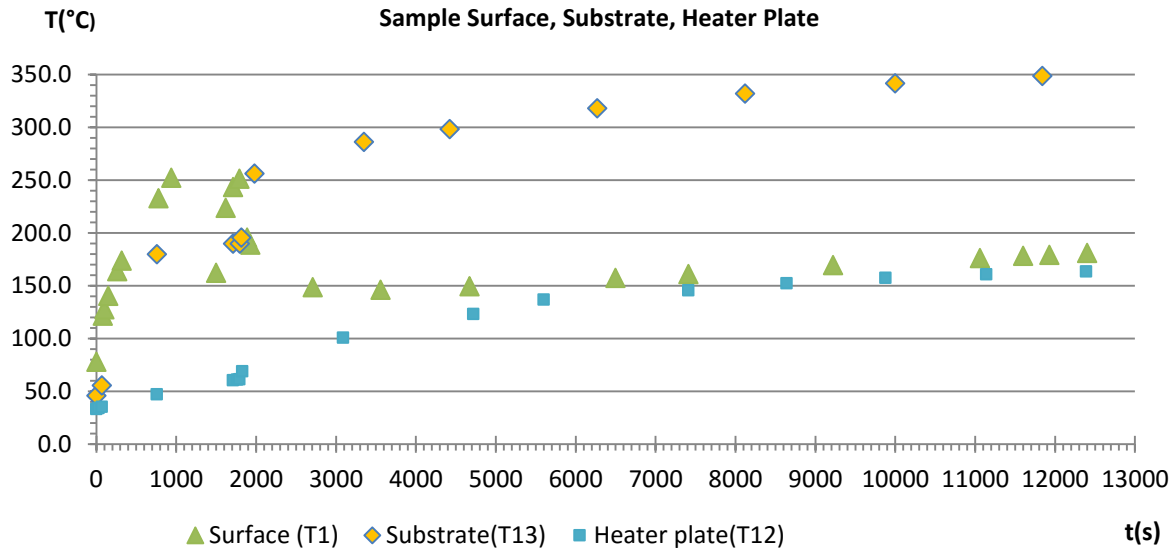

Fig. 38 - Temperatures on the surface of the sample (300 V), on the substrate (470 V) and on the heater plate (470 V), with the transverse c) hollow cathode configuration. Substrate temperature was measured with sample on the ceiling of the hollow cathode.

In this graph it can also be seen that the substrate (T13), with the sample placed on the ceiling of the hollow cathode, reaches a much higher temperature than the base plate. Also, there are no oscillations like the one measured at the sample's surface. This further supports that the temperature spike measured on the surface is rapidly dissipated.

From the experiments with the *cold samples,* it can be concluded that temperature, DC bias, cathode configuration, sample geometry and surface roughness; all have an effect on the final result. Also, DC bias and cathode configuration are limiting factors when it comes to lowering the temperature, since they both affect the amount of heat supplied to the workpiece. The experiments that had pre-heating only always reached a final stable temperature that seemed to be dictated by these two parameters. Therefore, if the initial temperature is closer to this final value, the process should have a more constant temperature throughout. This will maximize nitrogen diffusion without compromising the maximum temperature that the workpiece is subjected to.

Considering that the system (all cathode parts) reaches thermal equilibrium during the process, the temperature measured at the base plate is a rough approximation of the temperature of the sample. These temperature values are on the lower end of the precipitation heat treatment range (Fig. 3) and, therefore, far from the annealing range.

These results indicate that the process may be suitable for use in pre-treated alloys. It may also be possible to combine precipitation hardening and surface nitriding in only one

process, controlling the temperature and the duration of the nitriding process to achieve the desired aging effects.

5.3. SEM

SEM observations were performed in order to understand the effects of the nitriding process on the surface morphology and the development of the nitride layer throughout the process.

Fig. 39 shows the start of nitride formation on a mirror finished surface after pre-sputtering with $470\ \mathrm{V}$ at $400℃$. The AlN started forming on the grain boundaries in vertical columnar structures.

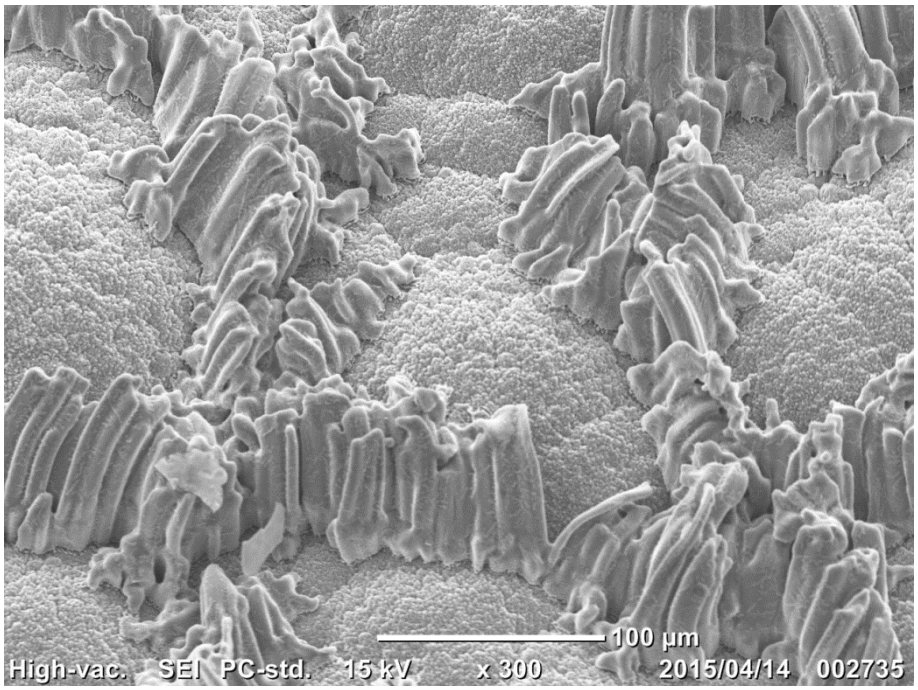

Fig. 39 – SEM micrograph showing the early stage of AlN formation on a mirror finished sample after pre-sputtering with $470\ \mathrm{V}$ at $400\ ℃$.

After growing from the grain boundaries, the AlN starts to cluster, forming cauliflower structures, like the ones shown in Fig. 40, covering the entire surface. These clusters continue to grow until they reach a morphology similar to the one seen in Fig. 41.

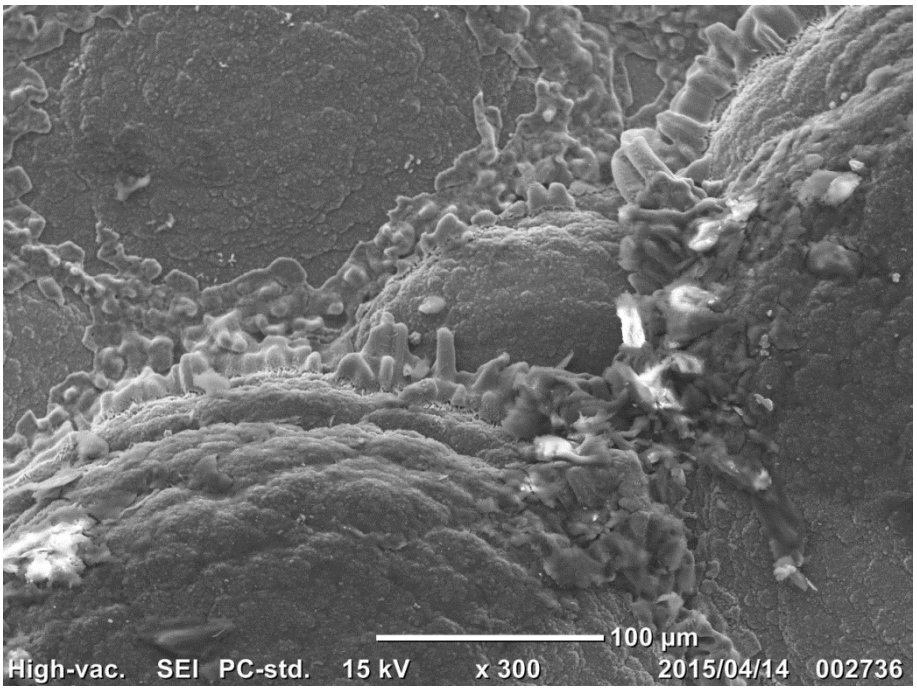

Fig. 40 – SEM micrograph showing nitride cluster formation.

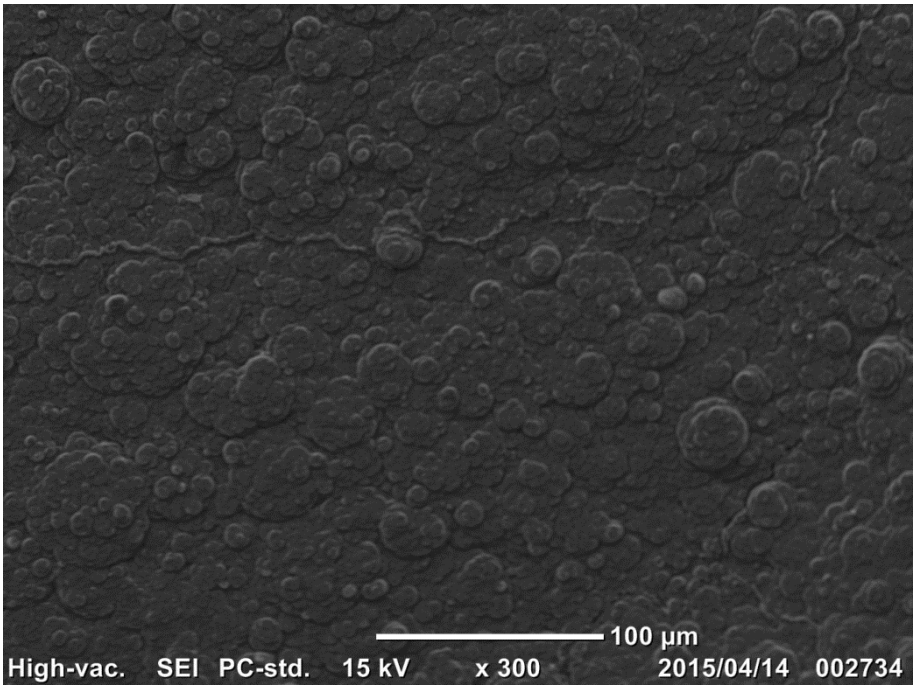

Fig. 41 – SEM micrograph showing a fully nitrided surface.

It was seen, experimentally that there is a processing time, in the *hot processed* experiments, after which the growth rate of the layer decreases drastically since an equilibrium on the concentration of nitrogen ions on the surface and on the surrounding

environment is obtained. This occurs after around 6 h of processing (or earlier, depending on the parameters).

These micrographs are examples of excessive nitride formation. The experiments shown above lead to irregular surfaces, very high roughness and delamination.

After tuning the parameters it was possible to obtain much smoother surfaces. Fig. 42 shows the SEM micrographs of two *cold processed* samples. One was polished with 2500 grade sandpaper, a), and the other was nitrided on the unpolished, as-cut surface, b).

The surface morphology of both samples is similar, though in Fig. 42b) the striations of the cut can still be distinguished. Lower nitrided formation rates, like the ones seen here, seem to have a more positive effect in keeping the original surface morphology.

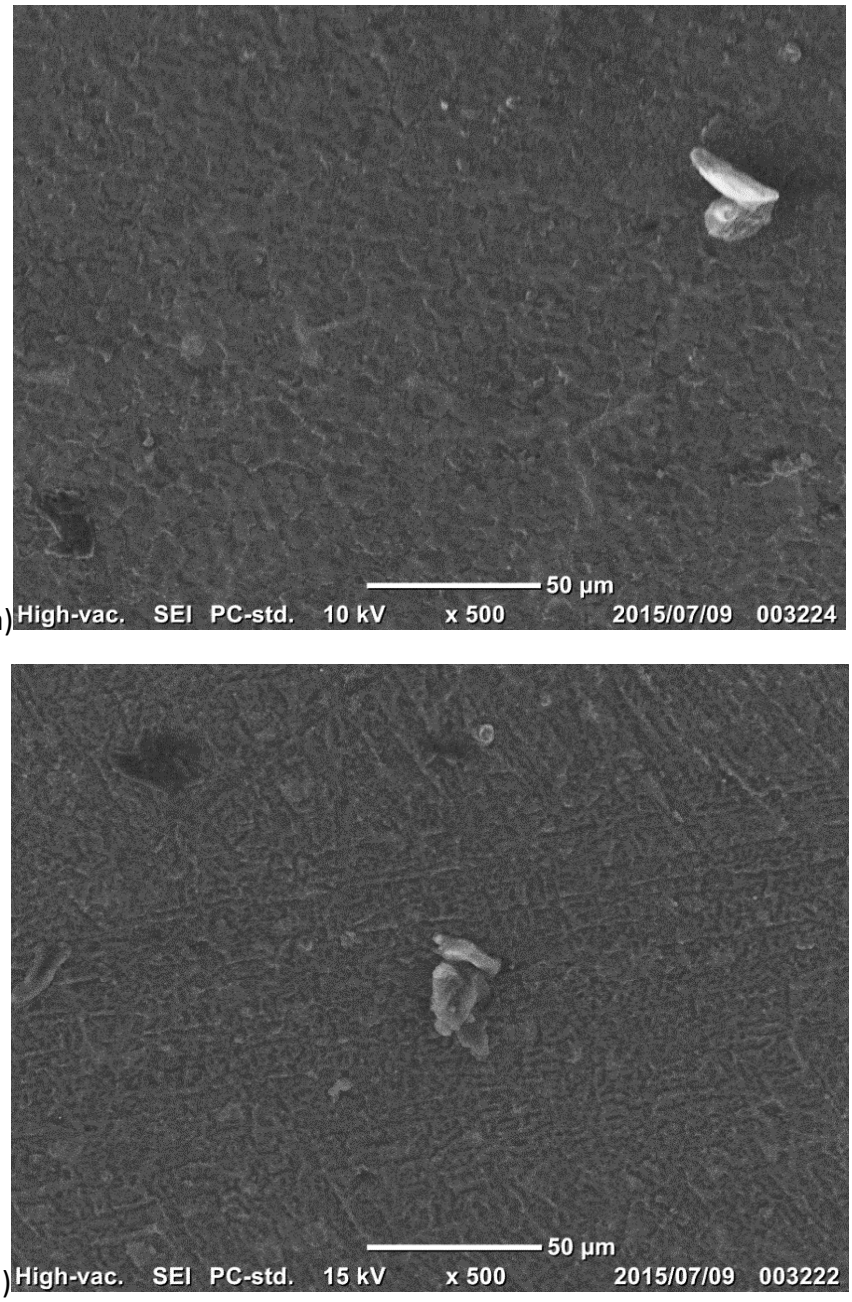

Fig. 42 – SEM micrographs showing two nitrided surfaces: a) starting from a polished surface, and b) starting from an unpolished, as-cut surface.

5.4. Electrical Characterization

Electrical characterization of this surface must be made by measuring *lift-off*, which varies with layer thickness, and electrical conductivity, which varies with the concentration of AlN in depth. Here they were analyzed separately to determine which one better

describes the nitrided surface. With this purpose, the EC system was tuned to show *lift-off* readings on the Im axis and electrical conductivity readings on the Re axis of the complex plane. The measurements performed on samples H91, H92 and H93 are plotted bellow in relative values.

Fig. 43 shows the measured values of *lift-off* on sample H91 for test frequencies of 100 kHz, 500 kHz and 1 MHz.

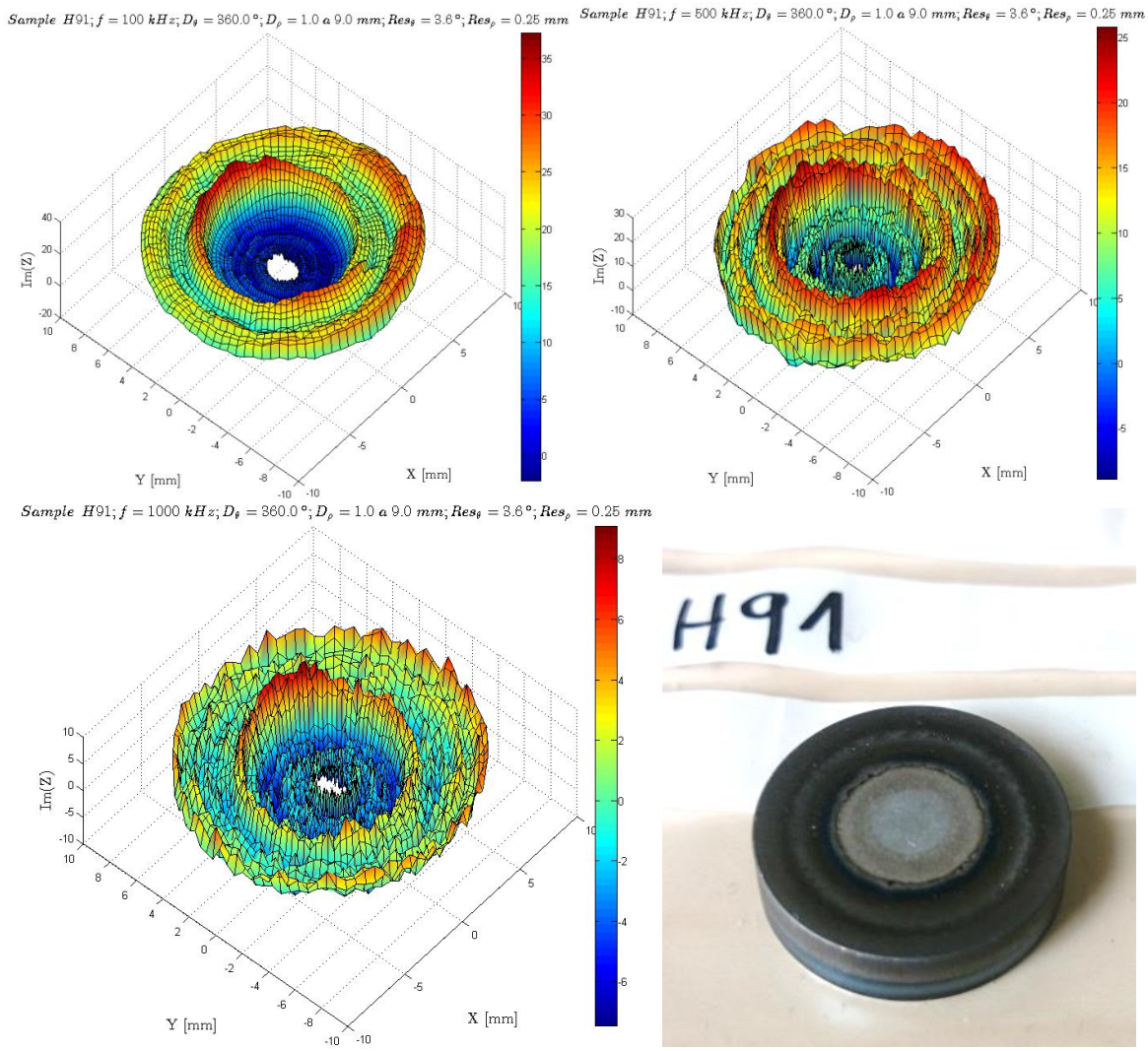

Fig. 43 – Eddy current 3D plot of sample H91; $Im(z)$ = lift-off.

As can be seen, the probe detected a steep increase in *lift-off* from the center to the darker nitrided region. Also, there are *lift-off* peaks on the transition to the nitrided area and on the edge of the sample which are coincident with the darker regions of the specimen. Between peaks there is a smaller *lift-off* which is coincident with the lighter

color. There is some lack of axisymmetry that may be explained by the direction of the gas/plasma flow during the nitriding process.

The measured values of *lift-off* on sample H92 at a frequency of $1\ \mathrm{MHz}$ are plotted in Fig. 44. Lower frequencies seemed to be unable to detect any *lift-off* on the nitrided area, except for the transition region.

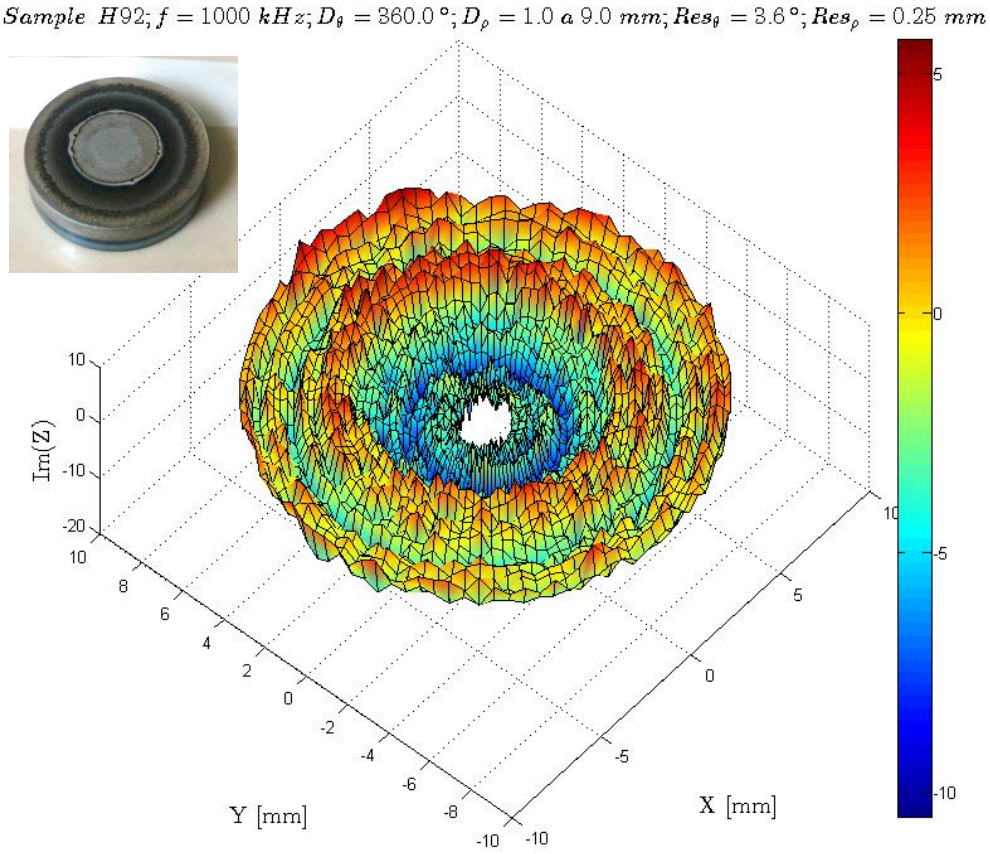

Fig. 44 – Eddy current 3D plot of sample H92; $Im(z)$ = lift-off.

Here it is still easy to distinguish a *lift-off* increase on the transition region but it is less steep. On the edge, there is a smaller peak that is only detected at $1\ \mathrm{MHz}$. These results suggest that the layer is thinner than on H91.

The measured values of *lift-off* for sample H93 at a frequency of $1\ \mathrm{MHz}$ are plotted in Fig. 45. Like in H93, lower frequencies seemed to be unable to detect the any *lift-off* on the darker region.

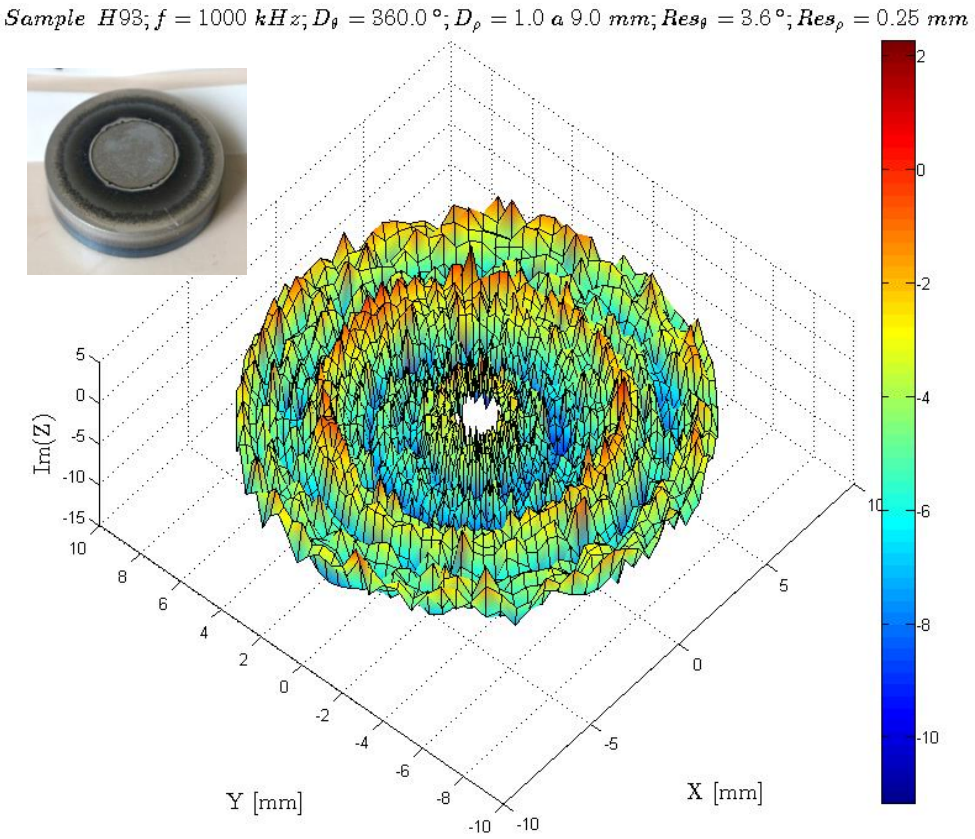

Fig. 45 – Eddy current 3D plot of sample H93; $Im(z)$ = lift-off.

Sample H93 shows much smaller *lift-off* values in comparison to H91 and H92, in agreement with a slightly lighter surface color. At this current frequency there is a non-zero measured lift-off on the center of the sample. These results suggest the layer may be too thin to be tested with this equipment.

The relative lift-off variations clearly follow the changes in color of each sample, as can be seen in Fig. 46.

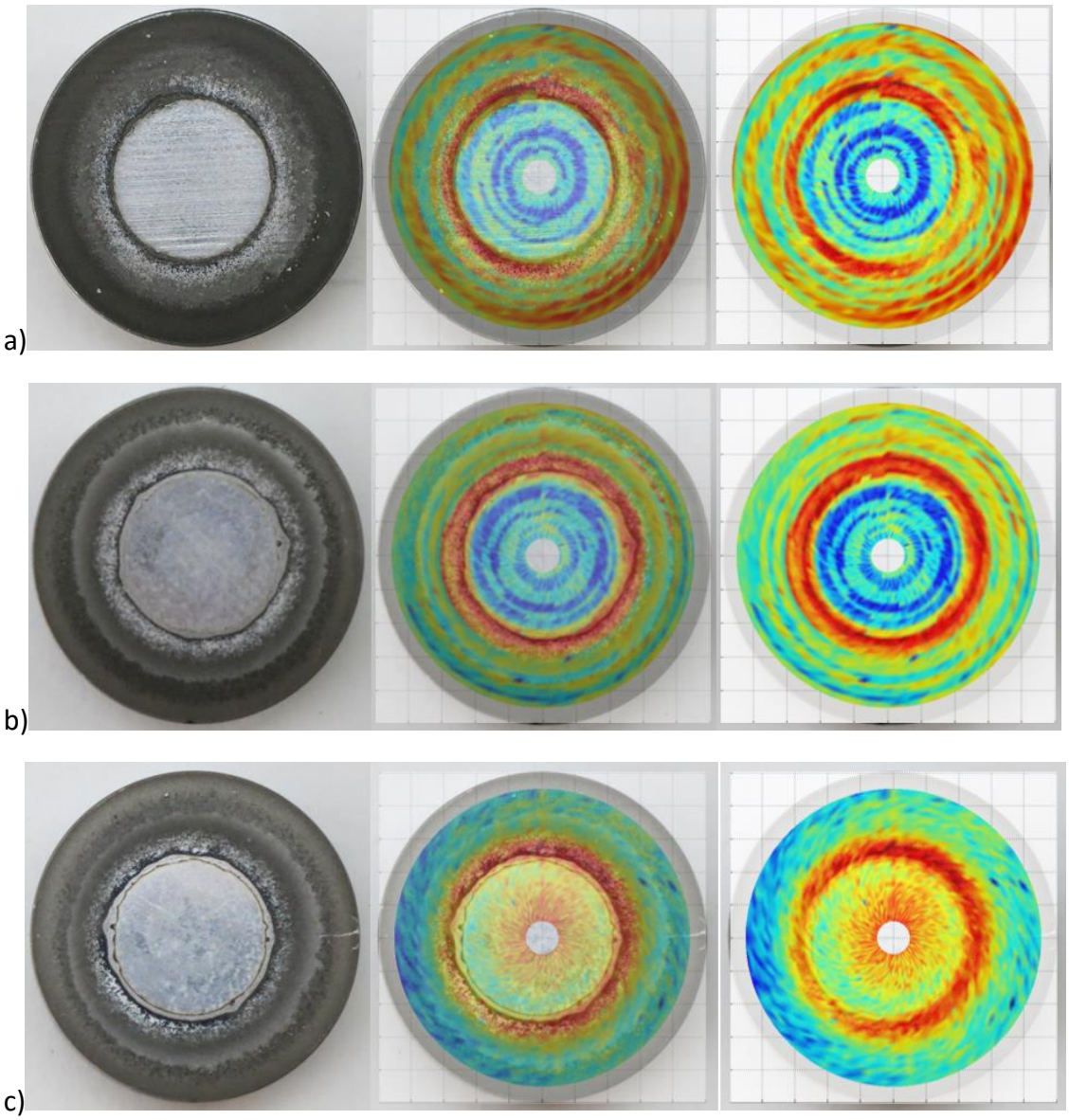

Fig. 46 – *Lift-off* at 500 kHz, overlapped with sample a) H91, b) H92, and c) H93.

Electric conductivity values of sample H91, H92 and H93, measured with the current frequencies that best described the surfaces, are plotted in Fig. 47. In the case of H91, with $100\ \mathrm{kHz}$ there was some edge effect and with $1\ \mathrm{MHz}$ there were no conductivity variations on the nitrided region.

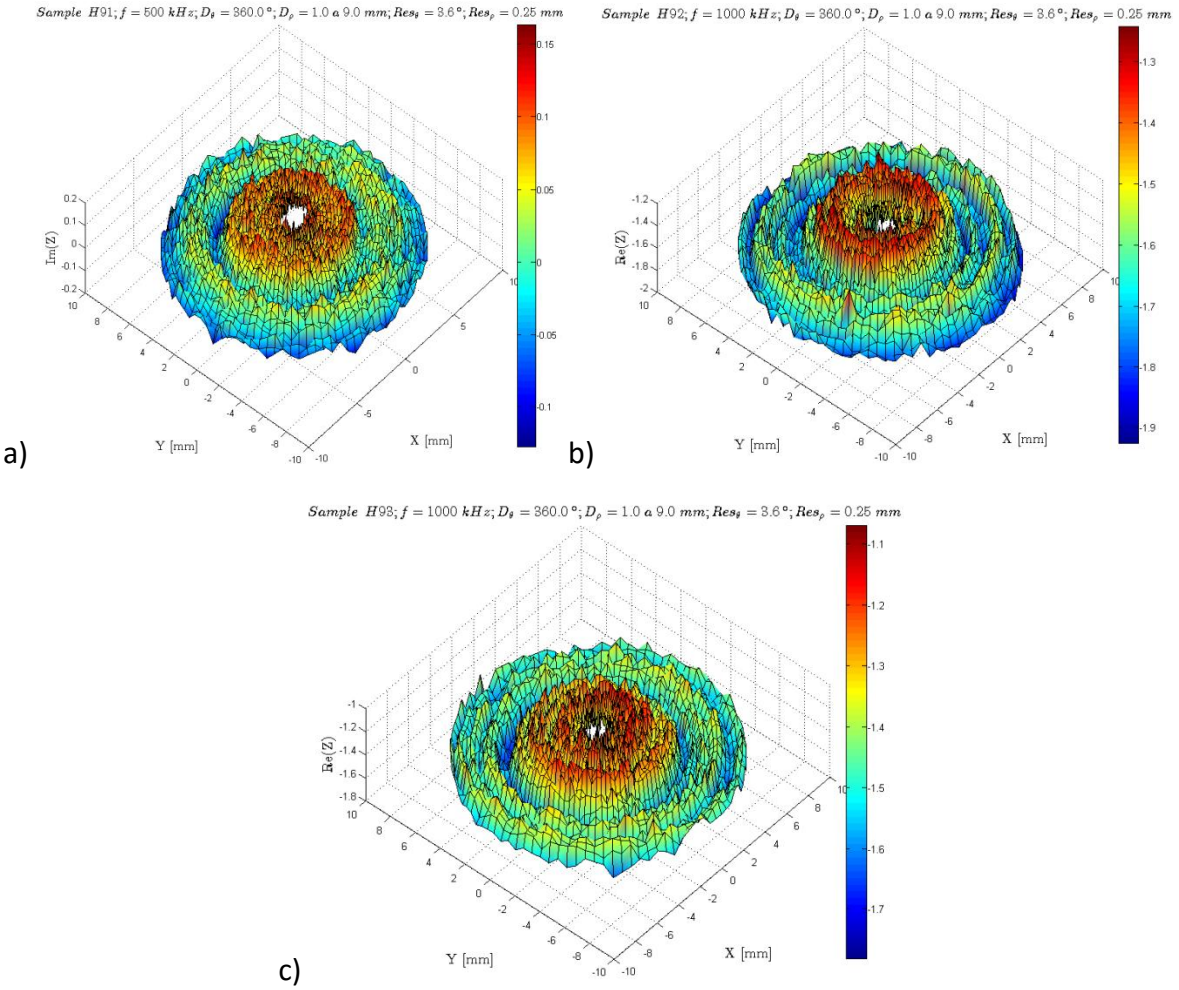

Fig. 47 – Eddy current 3D plot of samples a) H91, b) H92 and c) H93; $Re(z)$ = electrical conductivity.

As expected, the lowest conductivity was measured on the edge and on the transition zone, while between the two it is somewhat higher. This is consistent with the color of the sample and with the initial assumption that the nitriding is more intense where the plasma is brightest, namely on sharp edges.

5.5. Vickers Microindentation Hardness Tests

Hardness was measured in most samples however, in some, the indentations were too deformed or too small to be measured. Testing with small loads produced small indentations, impossible to see on the microscope available, while tests done with higher loads produced very distorted indentations, indicating that the layer was fully penetrated. Wear on the indenter tip may also have contributed to this matter. The hardness tests performed successfully are presented in Tab. 5.

Tab. 5 - Vickers hardness test values and respective loads. Locations of H6 indentations are shown in Fig. 48.

HV	Load(gf)	Indent.1	Indent.2	Indent.3	Indent.4	Indent.5	Indent.6
Not treated	100	132.4	131.6	130.8	137.2	129.1	
Not nitrided, 400℃	100	57.6	61.2	62.0	59.5	60.4	59.6
H3	100	61.2	60.9	60.1	61.5	59.6	59.5
	25	60.5	58.5	59.4	61.6		
H6(1)	100	117.0	117.4	101.5	104.3		
H6(2)	200	1176.0	1291.0	559.2	642.9	545.6	1045.0

As can be seen, there was a drop in hardness from the untreated to the not-nitrided at 400 ℃. This is due to stress relief, since the samples are produced by mechanical alloying.

Reference [11] reported a hardness value of 550 HV for a 25 gf load, which is much higher than the 60 HV measured in H3 with the same load and the same nitriding parameters. There seems to no significant increase in hardness in sample H3 compared to the not-nitrided at 400 ℃.

In specimen H6, even though there was much delamination, some surface areas were tested. The objective was to find some region, even if small, were there was a significant increase in hardness, closer to the theoretical values. The indentations were performed in the areas illustrated in Fig. 48 -– Locations of indentations of sample H6.Fig. 48.

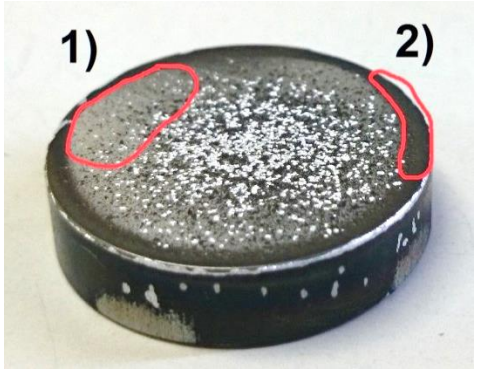

Fig. 48 -– Locations of indentations of sample H6.

The hardness of AlN was estimated in [10] to be around 1200 HV. The results of H6 support this estimate. Higher hardness values seem to be associated with more delaminated regions, as is clear in this sample.

6. FINAL CONCLUSIONS

From the study performed, it was seen that it is possible to nitride AA2011 at temperatures of 200 °C and lower, which is adequate for tempered alloys since no damage in base material properties is induced.

A thick AlN layer is easy to achieve, however, a thick layer is usually associated with excessive deposition and bad adhesion to the substrate. This is due to the low diffusion rate of nitrogen in the Al matrix, which is intensified as the processing temperatures decrease.

Homogeneous layers can be produced under the appropriate processing conditions. Apparently good quality nitride layers were achieved in this AA2011 alloy by modifying the cathode geometry.

Some geometries like holes and sharp edges were identified as being preferable sites for plasma concentration and, therefore, are responsible for creating heterogeneities in the nitrided surface.

In what concerns electrical characterization, the nitrided layers seem to be best described by measuring the *lift-off*, because the changes in surface color are accompanied by relative changes in the *lift-off* value. Direct measurement of the layer thickness must be performed to improve this type of evaluation. Electrical conductivity provides a less accurate profile and seems to be more affected by *edge effect*s at lower frequency.

Vickers hardness was measured in some samples but the values obtained were very low, in the order of 60 HV. This may be due to a very thin nitride layer that is penetrated by the indenter. In some samples the tests were inconclusive because of very distorted indentations. In one sample, where the deposited AlN was very thick, the maximum hardness measured was of about 1200 HV, which corresponds to the theoretical values, but delamination was observed.

Future work is needed to better understand the process under low temperature conditions.

In order to improve the knowledge of the processing parameters it would be interesting to do FEM simulations to determine the effect of RF and DC bias voltages on the intensity of the magnetic field; investigate how to obtain thicker layers with good adhesion at low temperatures (below 200 °C); and experiment with tempered specimens (e.g.T6) to see if the temper properties are preserved after the nitriding.

In terms of electrical characterization, it would be interesting to measure the thickness of the nitrided layers in cross-section and compare it with the eddy current evaluation, to search for a correlation between the two; and do similar tests in specimen of greater dimensions with the purpose of avoiding the nitriding heterogeneities produced on the edges and the *edge effect* of the eddy currents.

Nanoindentations and wear tests are essential in order to assess the mechanical properties of the nitride layer and to compare them with the eddy current tests.

REFERENCES

[1] ASM Handbook Committee, Vol.9, Metallography and Microstructures, ASM International, 2004.

[2] ASM Handbook Committee, Vol. 4, Heat Treating, ASM International, 1991.

[3] T. Fitz, "Ion Nitriding of Aluminum," PhD Thesis, 2002.

[4] P. Visuttipitukul, T. Aizawa and H. Kuwahara, "Advanced Plasma Nitriding for Aluminum and Aluminum Alloys," *Materials Transactions, Vol. 44, No. 12,* pp. 2695-2700, 2003.

[5] K. Taweesub, P. Visuttipitukul, S. Tungkasmita and B. Paosawatyanyong, "Nitridation of Al–6%Cu alloy by RF plasma process," *Surface & Coatings Technology,* vol. 204, p. 3091–3095, 2010.

[6] T. Ebisawa and R. Saikudo, "Formation of aluminum nitride on aluminum surfaces by ECR nitrogen plasmas," *Surface & Coating Technology,* Vols. 86-87, pp. 622-627, 1996.

[7] P. Visuttipitukul, T. Aizawa and H. Kuwahara, "Feasibility of Plasma Nitriding for Effective Surface Treatment of Pure Aluminum," *Materials Transactions, Vol. 44, No. 7,* pp. 1412-1418, 2003.

[8] L. Bardos, "Radio frequency hollow cathodes for the plasma processing technology," *Surface and Coatings Technology,* Vols. 86-87, pp. 648-656, 1996.

[9] M. Moradshahi, T. Tavakol, S. Amiri and S. Shayeganmehr, "Plasma nitriding of Al alloys by DC glow discharge," *Surface & Coatings Technology,* vol. 201 , p. 567–574, 2006.

[10] P. Vissutipitukul and T. Aizawa, "Wear of plasma-nitrided aluminum alloys," *Wear,* vol. 259, p. 482–489, 2005.

[11] T. Aizawa, S. Muraishi and Y. Sugita, "High Density Plasma Nitriding of Al-Cu Alloys for Automotive Parts," *Journal of Physical Science and Application,* vol. 4, pp. 255-261, 2014.

[12] F. Vacandio, Y. Massiani, P. Gergaud and O. Thomas, "Stress, porosity measurements and corrosion behaviour of AlN films deposited on steel substrates," *Thin Solid Films,* vol. 359, pp. 221-227, 2000.

[13] H. F. H. T. T. Arai, *Proceedings of the International Conference on Ion Nitriding,* pp. 37-41, 1986.

[14] N. Moncoffre, G. Barbier and E. Leblond, *Nuclear Instruments and Methods in Physics Research B,* vol. 140, pp. 402-408, 1998.

[15] D. Manova and P. Huber, *Journal of Vacuum Science & Technology A,* vol. 20, pp. 206-213, 2002.

[16] D. Manova, P. Huber, S. Mandl and B. Rauschenbach, "Surface modification of aluminium by plasma immersion ion implantation," *Surface and Coatings Technology,* vol. 128, pp. 249-255, 2000.

[17] T. Santos, P. Vilaça and R. Miranda, "Electrical conductivity field analysis for evaluation of FSW joints in AA6013 and," *Journal of Materials Processing Technology,* vol. 211, p. 174–180, 2011.

[18] T. G. Santos, R. M. Miranda, P. Vilaça and J. P. Teixeira, "Modification of electrical conductivity by friction stir processing of aluminum alloys," *Advanced Manufacturing Technology,* vol. 57, pp. 511-519, 2011.

[19] J. Bird, Electrical Circuit Theory and Technology, Oxford: Newnes, 2003.

[20] P. E. Mix, INTRODUCTION TO NONDESTRUCTIVE TESTING, John Wiley & Sons, 2005.

[21] R. Prakash, Non-Destructive Testing Techniques, New Age Science, 2009.

[22] T. G. Santos, "Ensaios Não Destrutivos por Correntes Induzidas: Desenvolvimento e Aplicação à Soldadura por Fricção Linear," PhD Thesis, 2009.

[23] T. Okada, M. Toriyama and S. Kanzaki, *Journal of Materials Science,* vol. 35, p. 3105–3111, 2000.

[24] C. A. Harper, Handbook of Materials for Product Design, Third Edition, McGRAW-HILL, 2001.

[25] "Engineering Toolbox," [Online]. Available: http://www.engineeringtoolbox.com/.

[26] ASM Handbook Committee, Vol.8, Mechanical Testing and Evaluation, ASM International, 1991.

[27] ASM Handbook Committee, Vol.13A, Corrosion Fundamental, Testing and Protection, ASM International, 2003.

[28] P. Visuttipitukul, T. Aizawa and H. Kuwahara, *Proceeding of ASM International Surface Engineering Congress,* 2003.

[29] K. Taweesub, P. Visuttipitukul, S. Tungkasmita and B. Paosawatyanyong, "Nitridation of Al–6%Cu alloy by RF plasma process".